EXPERIMENTAL SUPPORT FOR NUMERICAL SIMULATIONS OF ENERGY ABSORBING STRUCTURES

Stanisław Ochelski

Military Academy of Technology, Department of Mechanics and Applied Computer Science
Kaliskiego Street 2, 00-908 Warsaw, Poland
tel.: +48 22 683 95 48, fax: +48 22 683 71 52
e-mail: s.ochelski@wme.wat.edu.pl

Paweł Gotowicki

Military Academy of Technology, Department of Mechanics and Applied Computer Science
Kaliskiego Street 2, 00-908 Warsaw, Poland
tel.: +48 22 683 95 48, fax: +48 22 683 71 52
e-mail: p.gotowicki@wme.wat.edu.pl

Paweł Bogusz

Military Academy of Technology, Department of Mechanics and Applied Computer Science
2 Kaliskiego Street, 00-908 Warsaw, Poland
tel.: +48 22 683 95 48, fax: +48 22 683 71 52
e-mail: p.bogusz@wme.wat.edu.pl

Abstract

This paper presents experimental investigations of mechanical properties of materials used in the absorbing energy structures. Numerous experimental investigations are essential to develop a reliable numerical model of composite structures absorbing the impact energy. This model should correctly describe the dissipation of kinetic impact energy in the progressive crush process. Mechanical properties of composite materials like elastic modulus, strength, failure strains with influence of anisotropic properties are obtained experimentally. Different strength hypotheses are used for fibrous composites. The investigations on the complex stress state allow determining which of these theories describes the composite best. It was proved that both the matrix type and the structure of the composite have a very large influence on the SEA (Specific Energy Absorption), in particular on their crack propagation resistance. The dependence between the energy absorbed by a single energy absorbing element and a fragment of the structure absorbing the impact energy was discussed. Friction forces play the important role in the progressive crush of composites and they should be taken into account in developing a valid numerical model. Some authors state that the friction forces absorb 40% of the impact energy. The influence of failure strain rates on the absorbing energy capability, which is not clearly defined in the literature about composite structures, was also discussed.

Keywords: *polymer composites, energy absorbing structures, sandwich structures, specific energy absorption, experimental methods*

1. Introduction

Reliable numerical model of progressive crush for energy absorbing structures, correctly describing the kinetic energy dissipation process of the impact requires various data. They have to be obtained experimentally. Assuming progressive crush of the structure the following crush mechanisms have to be considered: splaying or lamina bending mode, fragmentation or transverse shearing crushing mode, local bending, brittle cracking and progressive wall folding. The detailed

description of the crushing modes can be found in [1]. The crushing modes of fibrous composites are complex and difficult to analyse because they are dependent on the structure and the type of composites.

The progressive crush process of energy absorbing elements is characterised by a complex stress field, so that their analysis is based on the hypotheses for anisotropic materials. Mechanical properties of composite plies, which knowledge is necessary for the hypotheses to be applied, have to be obtained in experimental research. In the elastic field of orthotropic composites the following factors are determined: elastic modulus in tension stress in three orthotropic directions (E_1^+, E_2^+, E_3^+), elastic modulus for the compressive stress in three orthotropic directions (E_1^-, E_2^-, E_3^-), shear modulus in shear stress for three orthotropic planes (G_{12}, G_{23}, G_{13}) and Poisson's ratio for three orthotropic planes (ν_{12}, ν_{23}, ν_{13}). In crush tests the following properties are obtained: tensile resistance in three orthotropic directions (R_1^+, R_2^+, R_3^+) compressive resistance in three orthotropic directions (R_1^-, R_2^-, R_3^-), shear resistance for three orthotropic planes (T_{12}, T_{23}, T_{23}), tensile failure strains (ε_1^+, ε_2^+, ε_3^+), compressive failure strains (ε_1^-, ε_2^-, ε_3^-), shear failure strains for three planes (ε_{12}, ε_{23}, ε_{23}).

To develop a realistic numerical model, it is necessary to use material characteristics obtained in dynamic tests: dependence stress-strain $\sigma(\varepsilon)$ for different strain rates as well as the relationship between the crush force and the displacement (specimen shortening) (P-Δl), obtained in a progressive crush test of the energy absorbing elements. This dependence is a fundamental relationship while verifying numerical models.

In specified above crushing modes of polymer fibrous composites, the fragmentation of the element together with crack propagation very often preceded with delamination plays a dominating role. It is necessary to examine crack propagation resistance of the composites because this factor has a large influence on their energy absorption capability. The better crack propagation resistance is the more impact energy the composite structure can absorb. While progressive crushing, friction force between composite plies and tensile machine support as well as friction force between composite plies both have a significant influence on the obtained value of the absorbed impact energy (EA).

The strain rates influence on amount of absorbed energy in progressive crush is not clearly defined for composite structures. Some publications present an increase of absorbed energy with a growth of deformation rates others show the opposite dependence. Therefore the necessity of experimental verification of this relationship is required.

Absorbing energy shell constructions are built as composite sandwich structures with different core shapes: tubes, truncated cones, sheet-metal sections, honeycomb structures, waved thin-walled structures. The cores are very often filled with foamed material.

Foamed materials can be obtained in various ways. The most often used materials are: polymers, metals, ceramics and glass. Foamed materials are characterized by large porosity therefore they are light. They have very low density, even smaller than 0.3 g/cm^3. During compressive loading of foamed materials various deformation mechanisms can occur: brittle crack, plastic deformations. Foamed materials demonstrate the isotropic dependence on loads and deformations as well as the small sensibility on the impact direction.

2. Determining of mechanical properties of the plastic materials

Polymer composites belong to a group of materials with rheological properties. Therefore they are sensitive to loading time. They are built from a matrix (resin) characterized with elastic, viscoelastic and plastic properties and fibre reinforcement with mainly elastic properties. Fig. 1 presents characteristics of typical fibres used in composite production. The stress unit is related to the mass of the fibre specific length.

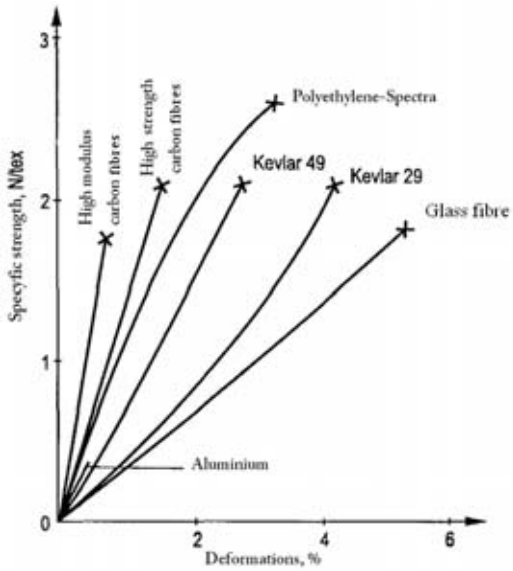

Fig. 1. Characteristics of typical fibres in tensile tests [2]

Presented examinations of the orthotropic composite mechanical proprieties covered epoxy resin E-53 reinforced with glass fabric STR-58. The composite specimens were made in the form of 6mm thick plates. They were examined according to norm PN-EN ISO-527-4 in static tests. All results of this research are shown in Tab. 1.

Numerical simulations of crack modes of the energy-absorbing constructions require material characteristics for various deformation rates. In the test of deformation rate influence on composite mechanical properties, there was used an orthotropic composite (which properties are presented in Tab. 1) and a unidirectional monotropic composite made of epoxy resin E-53 with glass fibre reinforcement.

In static, dynamic and creeping tensile tests performed for a wide range of deformation rate, deformation values were recorded until the specimen crush, which allowed obtaining mechanical properties of the examined composites. The results are presented in Fig. 2, 3 and 4 – as stress-strain curves.

Tab. 1. Mechanical properties of typical polymer composites

No.		Mechanical properties	Fabric reinforced glass/epoxy composite	Monotropic glass/epoxy composite	Mat reinforced glass/epoxy composite	Monotropic carbon/ epoxy composite	Fabric reinforced carbon/ epoxy composite	Unit
1	E_1^+	Tensile elastic modulus, direction 1	19.54	35.21	6.8	91.04	46.4	[GPa]
2	E_2^+	Tensile elastic modulus, direction 2	19.54	6.53	6.8	5.81	46.4	[GPa]
3	E_3^+	Tensile elastic modulus, direction 3	7.25	6.53	6.8	5.81	2.57	[GPa]
4	E_1^-	Compressive elastic modulus, direction 1	19.33	41.1	9.2	88.9	50.6	[GPa]
5	E_2^-	Compressive elastic modulus, direction 2	19.33	6.77	9.2	6.14	50.6	[GPa]
6	E_3^-	Compressive elastic modulus, direction 3	7.79	6.77	9.2	6.14	7.51	[GPa]
7	ν_{12}	Poisson's ratio, plain 1-2	0.143	0.311	0.27	0.27	0.14	[-]
8	ν_{13}	Poisson's ratio, plain 1-3	0.571	0.311	0.27	0.015	0.55	[-]
9	ν_{23}	Poisson's ratio, plain 2-3	0.571	0.44	0.27	0.53	0.055	[-]
10	G_{12}	Shear elastic modulus in plain 1-2	2.42	2.27	3.8	3.6	2.91	[GPa]
11	G_{13}	Shear elastic modulus in plain 1-3	2.92	2.27	3.8	1.6	4.3	[GPa]

No.		Mechanical properties	Fabric reinforced glass/epoxy composite	Monotropic glass/epoxy composite	Mat reinforced glass/epoxy composite	Monotropic carbon/ epoxy composite	Fabric reinforced carbon/ epoxy composite	Unit
12	G_{23}	Shear elastic modulus in plain 2-3	2.92	4.21	3.8	1.6	4.3	[GPa]
13	R_1^+	Tensile resistance in direction 1	311.7	665.1	83.5	1004.9	468.6	[MPa]
14	R_2^+	Tensile resistance in direction 2	311.7	3.5	83.5	24.1	468.6	[MPa]
15	R_3^+	Tensile resistance in direction 3	5.4	3.5	83.5	24.1	9.4	[MPa]
16	R_1^-	Compressive resistance in direction 1	306	412	170.9	578.7	375.2	[MPa]
17	R_2^-	Compressive resistance in direction 2	306	65	170.9	102.2	375.2	[MPa]
18	R_3^-	Compressive resistance in direction 3	258.1	65	170.9	102.2	327.7	[MPa]
19	T_{12}	Shear resistance in plane 1-2	38.4	8.8	83.3	39.1	57.03	[MPa]
20	T_{13}	Shear resistance in plane 1-3	59.8	8.8	83.3	12.3	20.6	[MPa]
21	T_{23}	Shear resistance in plane 2-3	59.8	61.1	83.3	12.3	20.6	[MPa]
22	ε_1^+	Failure deformation. tensile in direction 1	0.018	0.02	0.018	0.011	0.0101	[-]
23	ε_2^+	Failure deformation. tensile in direction 2	0.018	0.0006	0.018	0.0043	0.0101	[-]
24	ε_3^+	Failure deformation. tensile in direction 3	0.001	0.0006	0.018	0.0043	0.0029	[-]
25	ε_1^-	Failure deformation. compressive in direction 1	0.016	0.011	0.019	0.0065	0.0074	[-]
26	ε_2^-	Failure deformation. compressive in direction 2	0.016	0.013	0.019	0.0154	0.0074	[-]
27	ε_3^-	Failure deformation. compressive in direction 3	0.03	0.013	0.019	0.0154	0.057	[-]
28	γ_{12}	Failure deformation. shear in direction 1-2	-	0.035	0.029	0.035	0.034	[-]
29	γ_{13}	Failure deformation. shear in direction 1-3	-	0.01	0.029	0.0078	0.0043	[-]
30	γ_{23}	Failure deformation. shear in direction 2-3	-	0.01	0.029	0.0078	0.0043	[-]

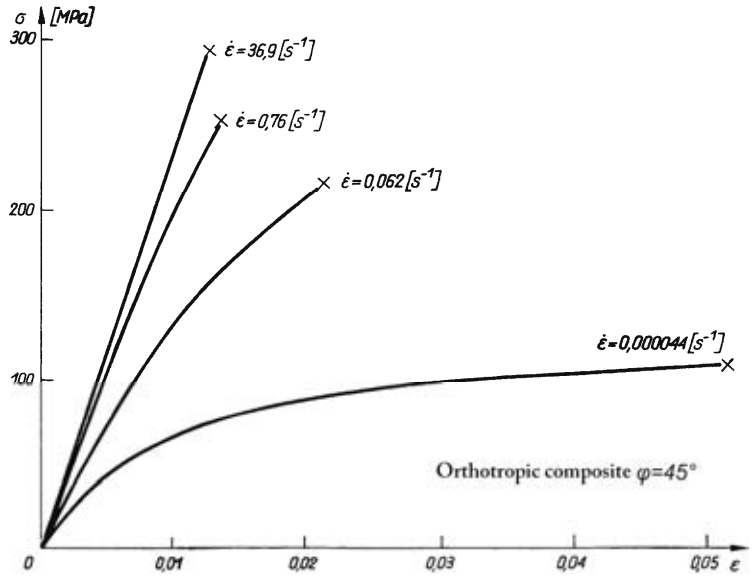

Fig. 3. The σ(ε) dependence of the epoxy composite reinforced with glass fabric for various strain rates in tensile tests at a 45° angle to the main orthotropic axis [4]

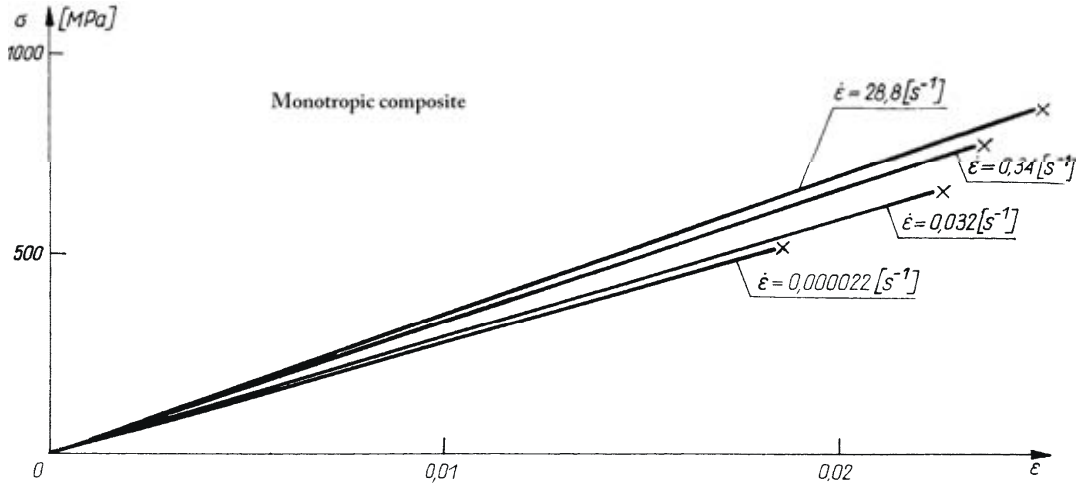

Fig. 4. The σ(ε) dependence of the epoxy composite reinforced with glass fabric for various strain rates, in tensile tests along the fibre direction [4]

The comparison of the results obtained for both orthotropic and monotropic composites illustrates a significant influence of filament orientation on mechanical properties with strain rates variations. The monotropic composite loaded along the fibres is little sensitive to strain rate variations. The orthotropic composite in tension at a 45° angle to the matrix direction demonstrates considerable variations of the properties with deformation rate changes. Variations of the tensile strength and the elastic modulus for the given composites are presented in Fig. 5 and 6.

Fibre composites in complex stress states behave completely different than isotropic materials. The paper [5] presents experimental verification of the following strength hypotheses: Małmajster, Goldenblat-Kopnow, Marin-Hoffman and Azzi-Tsai hypotheses. Tube specimens were prepared from epoxy resin with glass fibre reinforcement, using transverse-longitudinal winding method, with transverse to longitudinal fibres ratio equal to 1.46:1. The specimens had the following dimensions: total length 400 mm, gauge length 200 mm, internal diameter 108 mm and wall thickness 3.5 mm. The pressure applied inside the first specimen caused a plain stress state. The second state was performed by applying pressure with tensile or compressive load simultaneously.

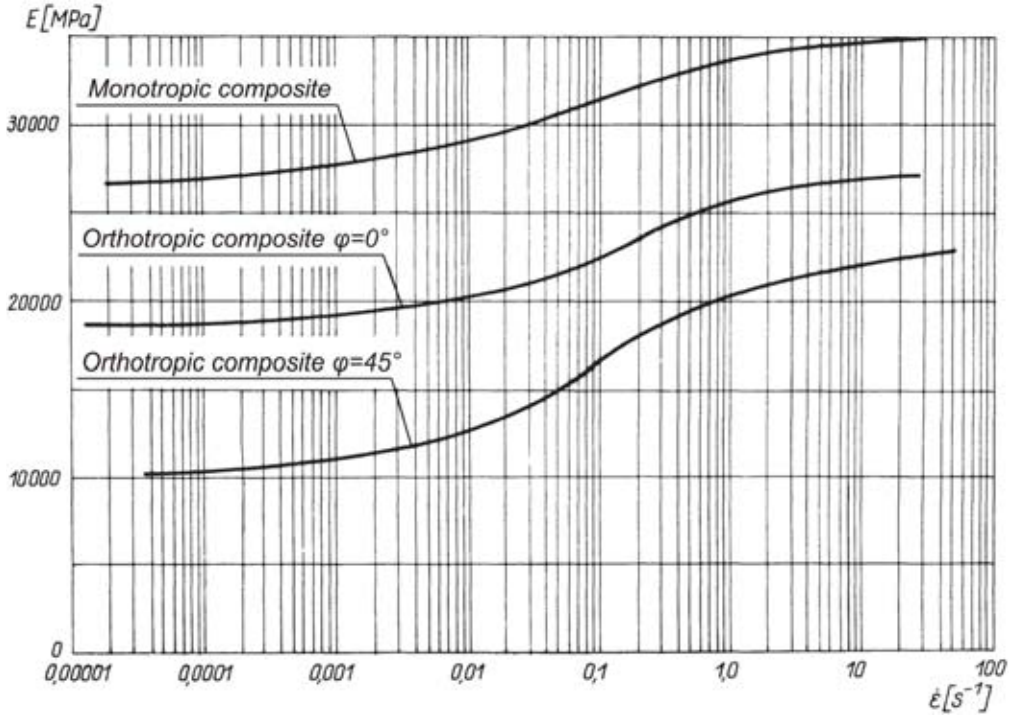

Fig. 5. Dependence of tensile modulus of elasticity on deformation rate for the examined composites [3]

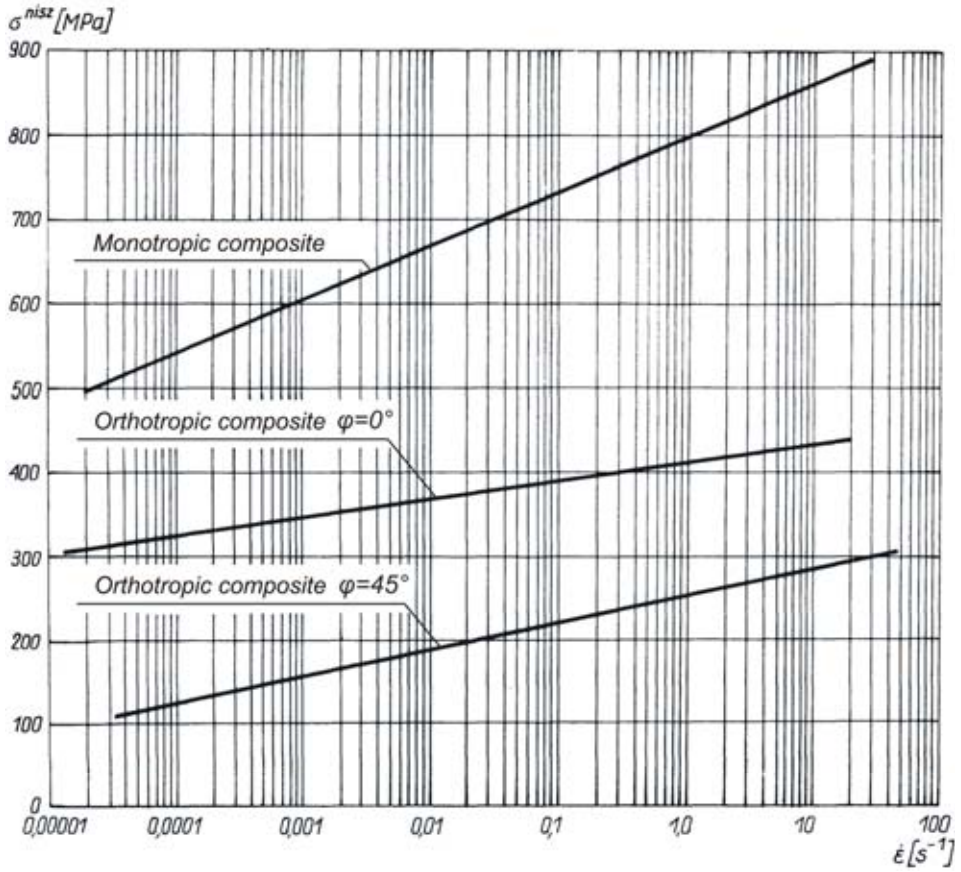

Fig. 6. Dependence of tensile strength on deformation rate for the examined composites [3]

The third state was made by applying torsion and tensile. Experiment results are presented in Fig. 7. They are described by the criteria specified above. The authors of the paper [5] state that the Małmajster hypothesis describes obtained results of the examined composites the most accurately. Asymmetry of the graphs comes from a different composite strength in tension and compression.

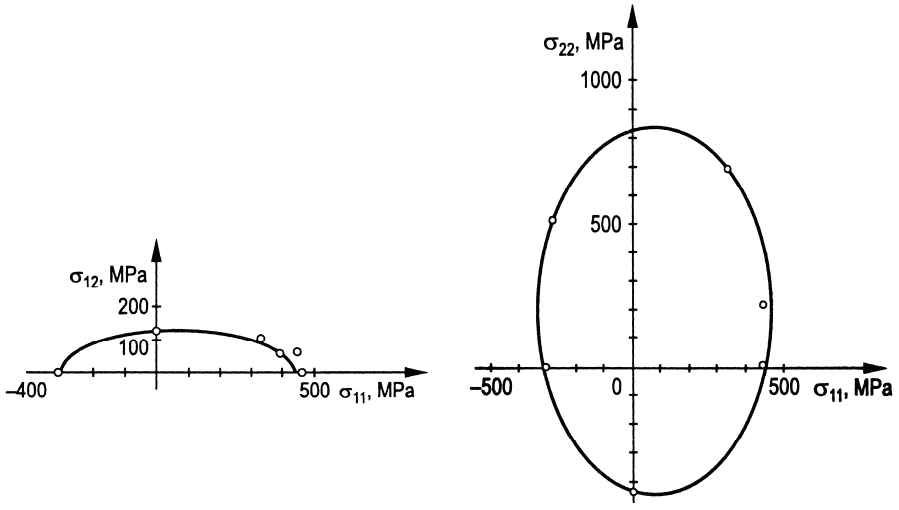

Fig. 7. Strength curves of glass fabric/epoxy composite in plane stress state [5]

The paper [6] presents research in a complex stress state of an epoxy composite reinforced with unidirectional glass fibres. There were examined tube specimens with 68 mm internal diameter in its fastening part, 50 mm external diameter, 1-4 mm thickness in gauge part. In tensile and

compression tests, there were examined flat specimens. Complex load states were realized by simultaneous applying torsion with tension or compression and by applying biaxial compression or biaxial tension. The results of the unidirectional reinforced composite specimens are presented in Fig. 8. It can be noted that monotropic composites have very strong anisotropic properties.

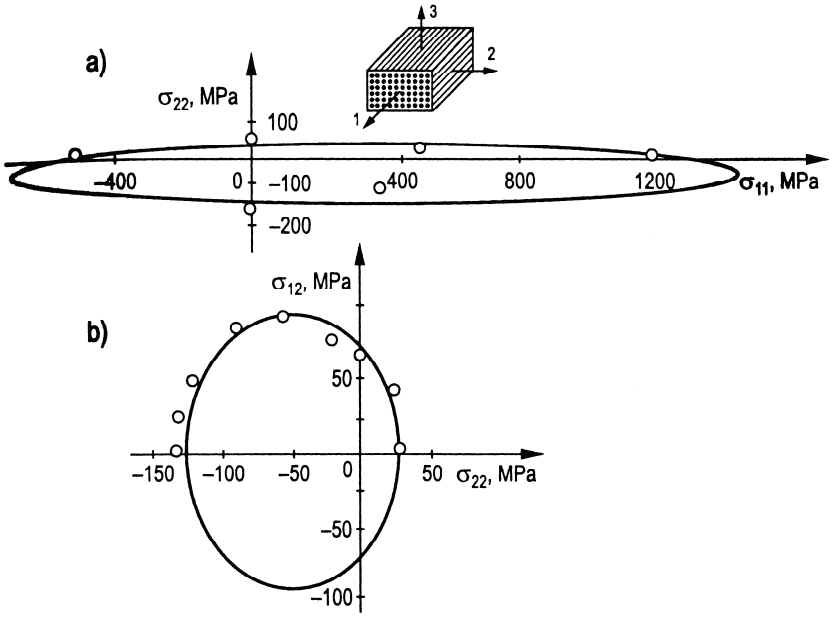

Fig. 8. Experimental results of the epoxy composite reinforced with unidirectional glass fibres in plain stress field [6]

3. Crack propagation resistance of composites

Crack propagation and delamination occurring under low loading essentially influences the absorbing energy ability of the composite structures. The analysis of different composite kinds and structures requires carrying investigations of crack propagation resistance, which is very low in the orthogonal direction to fibres and plies. Crack propagation in laminar composites usually occurs between the plies (delamination), therefore fibres inserted orthogonally to this plies increase resistance to delamination. Anisotropic properties and a type of the matrix have a large influence on crack resistance of the composites.

Energy release rate G_i determines material resistance to the crack growth. Index "i": indicates various crack loading modes: i = I – crack tearing, i = II – longitudinal shear, i = III – transverse shear. The energy release rate G_i for orthotropic materials is defined as follows:

$$G_I = K_I^2 \sqrt{\frac{S_{11}S_{22}}{2}} \left[\sqrt{\frac{S_{22}}{S_{11}} + \frac{2S_{12} + S_{66}}{2S_{11}}} \right]^{1/2}, \tag{1}$$

$$G_{II} = K_{II}^2 \frac{S_{11}}{\sqrt{2}} \left[\sqrt{\frac{S_{22}}{S_{11}} + \frac{2S_{12} + S_{66}}{2S_{11}}} \right]^{1/2}, \tag{2}$$

where:

K_i - stress intensity factor,
S_{ij} - susceptibility matrix coefficients in constitutive equation for orthotropic materials.

The stress intensity factor K_I is determined from the following equation:

$$K_I = \sigma\sqrt{\pi a}\ . \tag{3}$$

Analogically, for the loading mode II:

$$K_{II} = \tau\sqrt{\pi a}\,, \tag{4}$$

where "a" is defined as a half-length of the initial crack.

Experimental investigations of crack resistance can be made on standard tensile machines. A precise description of the specimens and fixtures used in the experiments for all crack-loading modes (I, II, II or mixed modes) can be found in [4].

In paper [7] you can find a fixture with a specimen used for I, II and I+II loading mode investigations. Fig. 9 presents a scheme of this fixture. A loading mode I is obtained when $\alpha = 90°$, mode II – $\alpha = 0$ and a mixed mode with different I to II mode ratios when $0° < \alpha < 90°$. The wheel plate has an external diameter of 203 mm and the thickness of 13.2 mm. The specimen has a notch on one of its edges (initial crack).

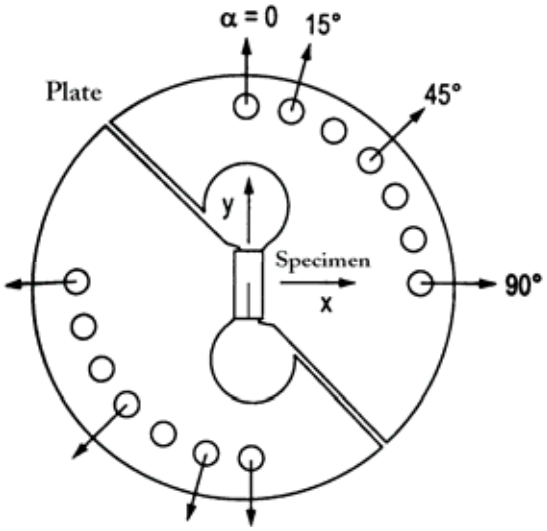

Fig. 9. Universal ARCAN fixture allows acquiring different crack loading modes [7]

The specimens used in ARCAN fixture had initial crack on one of their edges. The specimen dimensions were as follows: length L = 38.1 mm, width B = 13.2 mm, thickness 2h = 12.7 mm. Load ratio was equal to 0.5 mm/min. Applying load in different points of the plate generates the following stress components in the specimen:

$$\sigma_x = \sigma \sin\alpha\,, \tag{5}$$

$$\tau_{xy} = -\sigma \cos\alpha\,, \tag{6}$$

where σ is quotient of force to cross-sectional area of the specimen and α is the angle between specimen symmetry axis and loading direction.

Stress intensity factors K_I and K_{II} were calculated from the following formulas:

$$K_I = \sigma_x \sqrt{\pi a} f_1\left(\frac{a}{L}\right), \tag{7}$$

$$K_{II} = \tau_x \sqrt{\pi a} f_2\left(\frac{a}{L}\right), \tag{8}$$

where:

a - crack length,

L - specimen length,

f_1, f_2 - coefficients correcting the finished specimen geometry compared to the infinite shield.

$$f_1 = 1{,}12 - 0{,}231\frac{a}{L} + 10{,}55\left(\frac{a}{L}\right)^2 - 21{,}27\left(\frac{a}{L}\right)^3 + 30{,}39\left(\frac{a}{L}\right)^4, \tag{9}$$

$$f_2 = \frac{1{,}22 - 0{,}56\frac{a}{L} + 0{,}085\left(\frac{a}{L}\right)^2 + 0{,}18\left(\frac{a}{L}\right)^3}{\left[1-\left(\frac{a}{L}\right)\right]^{\frac{1}{2}}}. \tag{10}$$

The obtained stress intensity factors were used to determine energy release rates G_I and G_{II} from formulas (1) and (2), in witch S_{ij} are the components of the susceptibility matrix.

3.1. Influence of anisotropic properties

The performed investigations of fibre-reinforced composites (monotropic) proved that cracks propagate along the fibres independently of the applied loading mode (I, II or I+II). In [8] epoxy composites reinforced with continuous graphite filaments were studied. Specimens had angle between initial crack and direction of filaments equal to: 0°, 90° and 60°. Fig. 10 presents the dependence load-displacement for all investigated crack-to-fibre orientations.

The specimens with 0° fibre orientation crushed catastrophically after the load had reached its maximum value. Moreover, samples with 60° fibre orientation exhibited a constant crack growth or catastrophic crush. In specimens with 90° fibre orientation crack developed together with loading increase. The maximum load at which crack initiation appears is the critical load.

By inserting into composite reinforced in x, y plane with crossed fibres $[(0/90)_n]_s$ (2k-reinforced bidirectionally) fibres perpendicularly to this plane, we can receive a composite orthogonally reinforced (3k-tridirectional). Investigations determining resistance on crack growth in DCB test proved ten times larger resistance on crack development in 3k-composite tests compared to 2k-composite. Fibres inserted into 2k-composite perpendicularly to the layers raise tensile resistance and elastic modulus in the axial direction; however reduce stiffness and strength in x, y plane.

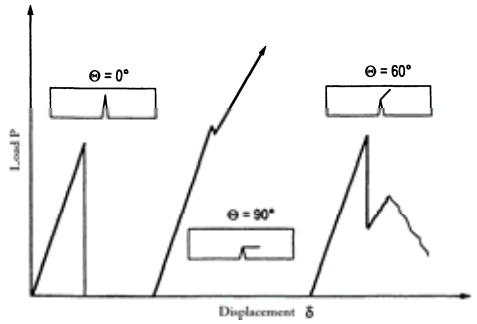

Fig. 10. Schematic illustration of P-δ dependence for the specimens with 0°, 90° and 60° fibre orientations [8]

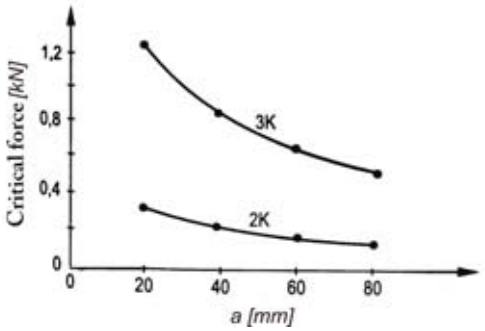

Fig. 11. Comparison of P_c-dependence for the 2k and 3k composites [9]

Mechanical proprieties of the composite matrix have a large influence on the crack growth resistance. It was proven that the more brittle matrix is, the less crack resistance is. The investigation on the influence of a matrix type and loading modes (I, II, I+II) on crack growth (delamination) under static and periodically variable loading was presented in [10]. There were examined three different composites with unidirectional fibres: T300/3100 (graphite/bismaleid matrix), IM6/R6376 (graphite/epoxy resin) and AS4/APC-2 (graphite/PEEK). DCB, ENF, CLS specimens were investigated in: I, II and I+II crack loading modes.

Critical energy release rate G_c was defined in static tests for all composites under mixed loading modes (Fig. 12). The largest resistance on cracking was obtained for a thermoplastic polyetheretherketone matrix, while the smallest resistance was noted for a brittle bismaleid polymer matrix (heat-hardened).

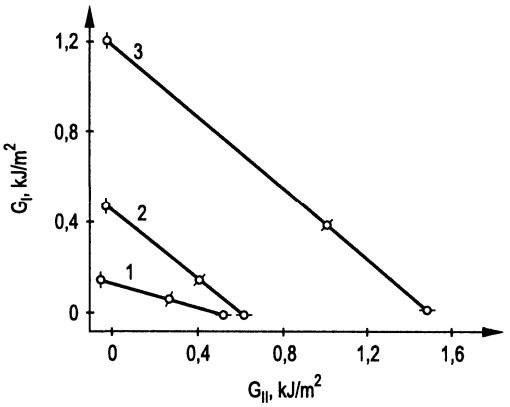

Fig. 12. G_I-G_{II} dependence for the composites with different matrix types: 1 – T300/3100, 2 – IM6/R6376, 3 – AS4/APC-2 [10]

4. Determining of friction factors

In numerous numerical simulations it is necessary to take into account friction force. The paper [11] contains experimental investigations of friction force and friction coefficients for composite––metal and composite ply–composite ply friction in load conditions similar to the progressive crush.

The investigation was conducted on universal tensile machine INSTRON 8802 with additional gauge head, which allowed to measure transverse force T. The equipment consisted displacement sensor, strain gauge bridge with the computer which recorded data. The coefficient of friction was defined as the ratio of transverse force to normal force loading down the specimen.

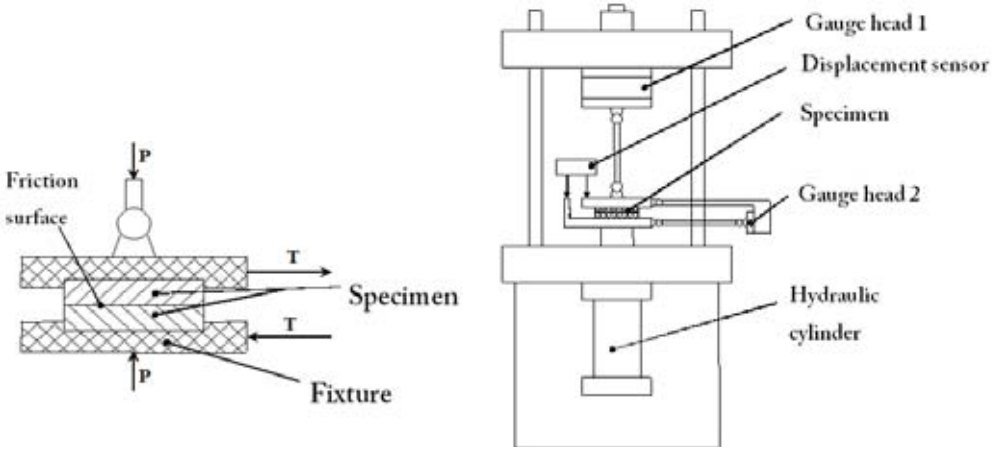

Fig. 13. Scheme of the test equipment used in the investigations of friction factor between two composite plies

The specimens examined in the composite ply-composite ply friction test were made of an epoxy composite reinforced with glass fabric. The friction force was measured between two surfaces formed by splitting a composite plate along one of its edges. The specimen was loaded with a force P normal to the motion direction. Applying force T caused the examined surfaces to move relatively to each other (Fig. 13). PC computer recorded forces P and T as well as a relative displacement between the surfaces. These parameters were used to calculate the friction factor between the examined surfaces. A determined coefficient of friction between two surfaces of the crushed composite is equal to 0.35 ±0.1.

In the next step the cinematic coefficient of friction between the crushed specimen surface and a steel plate of the tensile machine was obtained. The investigation was performed on the equipment described above. However, the test was applied to a tube made of glass fabrics/epoxy composite. The specimens had an internal diameter of 39.3 mm and were loaded with axial force P. Force T was applied perpendicular to the plate surface of the tensile machine – Fig. 14. The friction coefficient obtained in this test was equal to 0.32 ±0.03.

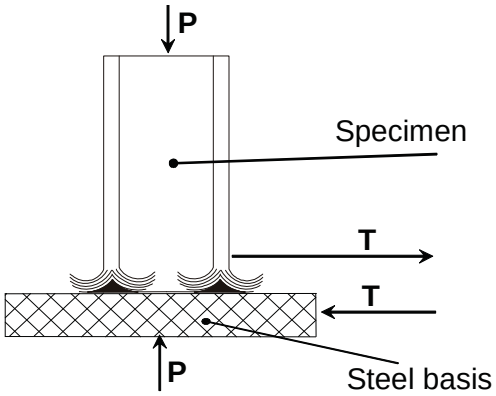

Fig. 14. Scheme of the test arrangement used in the investigations of friction factor between composite crushed structure and the steel basis

5. Rheological properties of polymer composites

Rheological effects have a large influence on mechanical properties of polymer composites, such as elastic modulus and strength. However they have limited influence on the energy absorption ability.

Classic creep curve – Fig. 15, which shape depends on the composite structure and kind, illustrates quantities related to the creep process. Total deformations during the creep can be described by the formula:

$$\varepsilon(t) = \varepsilon^{o} + \varepsilon^{p}(t). \tag{11}$$

In this relationship, there are:

ε^{o} - immediate strains, which can consist elastic strains $\varepsilon^{s} = \sigma / E$ and inelastic strains ε^{ns},

ε^{p} - creep strains which are dependent on time and can be divided on residual strains $\varepsilon^{r}(t)$ and partly reversible strains $\varepsilon^{cn}(t)$.

After specimen unload in given moment t_1 (Fig. 15) strains decrease immediately to the value approximately equal to ε^{s}. Strains $\varepsilon^{p}(t)$ can be reversible entirely or partly. In case when $\varepsilon^{p}(t)$ is not reversible totally, permanent strains ε^{t} are formed from residual strains ε^{r}. Permanent strains are defined as value of the asymptote to which the reverse curve approaches when test time tends to infinity $(t \to \infty)$.

Presented discussion of creep effects leads to the following conclusions: strain growth inside the material is the result of simultaneous deformation processes: elastic, viscous (relaxation) and plastic (slip).

A tri-parameter standard model (two springs and a damper) well describes the rheological processes. It takes into account immediate elastic strains, creep strains and the strain of viscoelastic reverse.

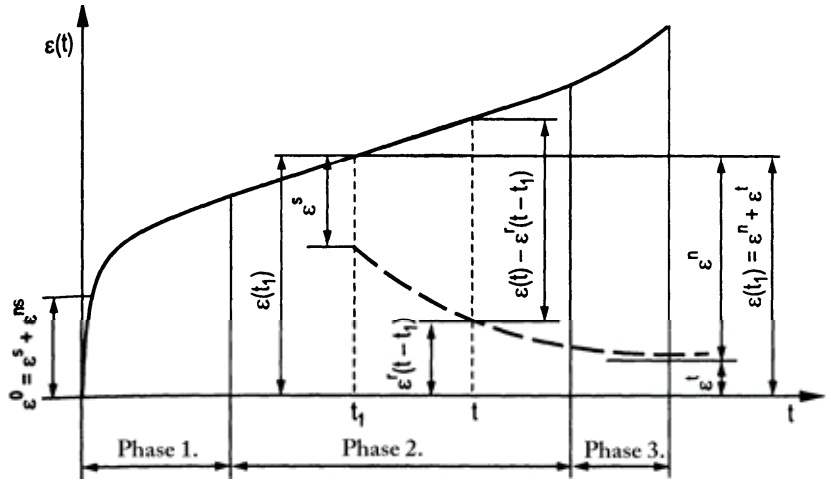

Fig. 15. Strains in the creep test

Anisotropic proprieties of the composites not only considerably change the strain value in dependence on loading time and stresses, but also the character of creep curves. Creep curves, which are presented in Fig. 16 and 17 [4], were obtained during tensile load of orthotropic composites in the fabric warp direction ($\varphi = 0$) and in 45° direction to the fabric warp of the orthotropic material. They show very different values of strains for the same time of loading. Therefore we can state that the orthotropic composite has strong anisotropic proprieties. The composite loaded in $\varphi = 0$ reveals a tendency to large immediate strains (elastic) and very small creep strains. However, when loaded down at an angle $\varphi = 45°$ – there are small immediate strains and large creep strains so that large viscoelastic and permanent strains occur.

The results of the monotropic composite creep tests presented on Fig. 18 confirm its high elastic proprieties and very small rheological strains, which should cause small impact of the strain ratio variations on Specific Energy Absorption (SEA).

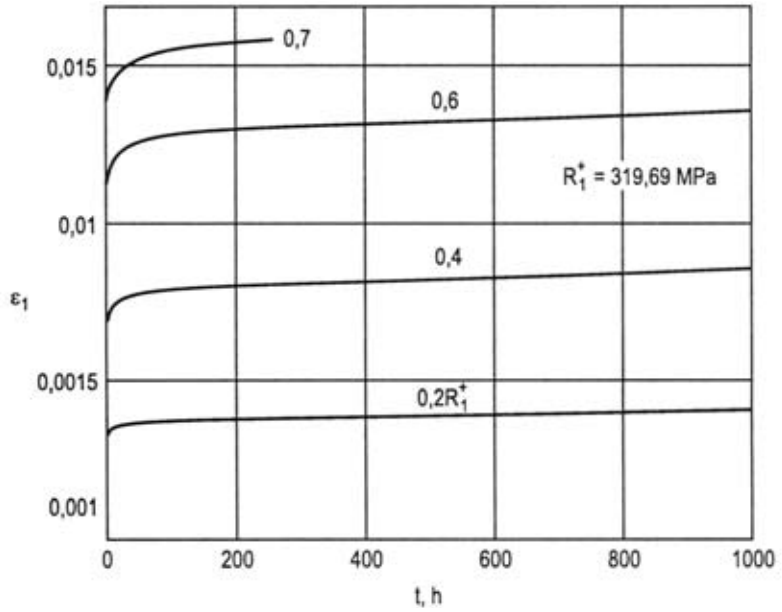

Fig. 16. Creep curves of the orthotropic epoxy composite reinforced with glass fabrics stretched in the fabric warp direction [4]

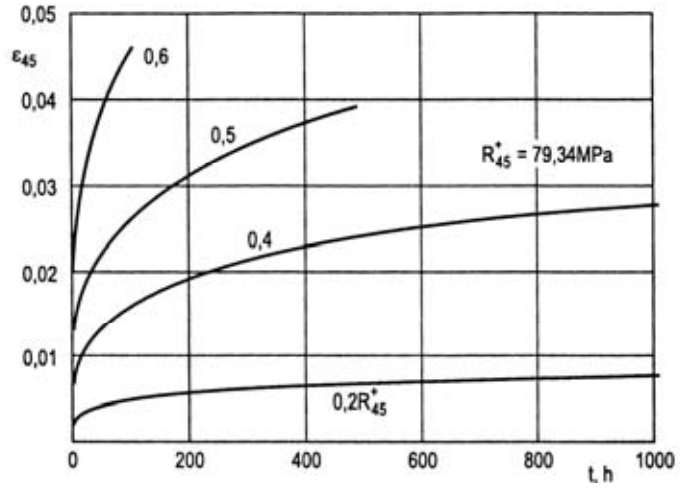

Fig. 17. Creep curves of the orthotropic epoxy composite reinforced with glass fabrics and stretched at an angle of 45° to the fabric warp [4]

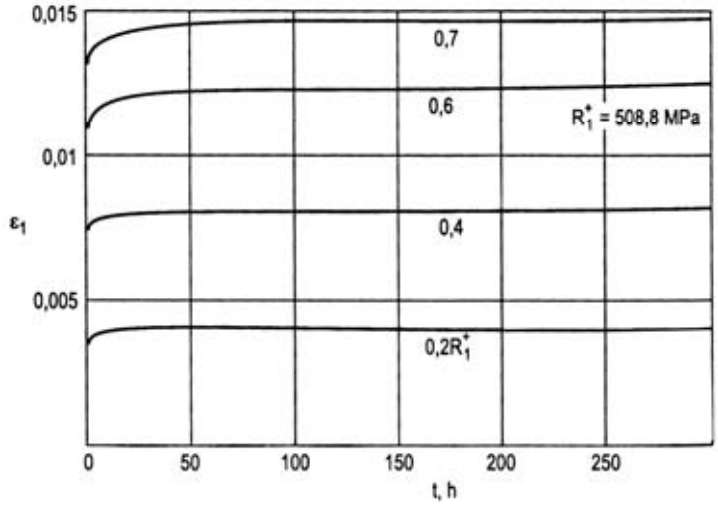

Fig. 18. Creep curves of the monotropic epoxy composite reinforced with unidirectional glass fibres [4]

Based on the results presented on Figs 16-18 you can conclude that the strength and the elastic modulus of the polymer composites are very sensitive to strain rates. The rheological investigation results proved that the polymer composites loaded down at an angle of 45° revealed large viscoelastic strains. We will check then how specified polymer composite characteristics influence the amount of SEA.

6. Load ratio influence of energy absorbing constructions on SEA

The influence of failure strain ratio on absorbing energy ability is not unequivocally defined in publications related to energy-absorbing composite structures. Various authors prove that with the increase of the strain ratio the energy absorbed by the composite rises. However, several publications present the opposite effect or that the absorbed energy does not depend on the strain ratio. It should be noted that they do not take into account the specific proprieties of different composite structures. It is very difficult to formulate general conclusions. Yet it is clear that the crush mode of the polymer composites can vary in dynamic and static loading conditions, as well as that the polymer composites behaviour factor plays an important role in this matter.

On Fig. 19, there were presented the results of investigations from publication [13]. Those data convince that the loading rate change in the range of 0.01-25 m/s causes insignificant SEA growth noted for the carbon/epoxy composite. This composite has high elastic proprieties and does not exhibit viscoelastic strains.

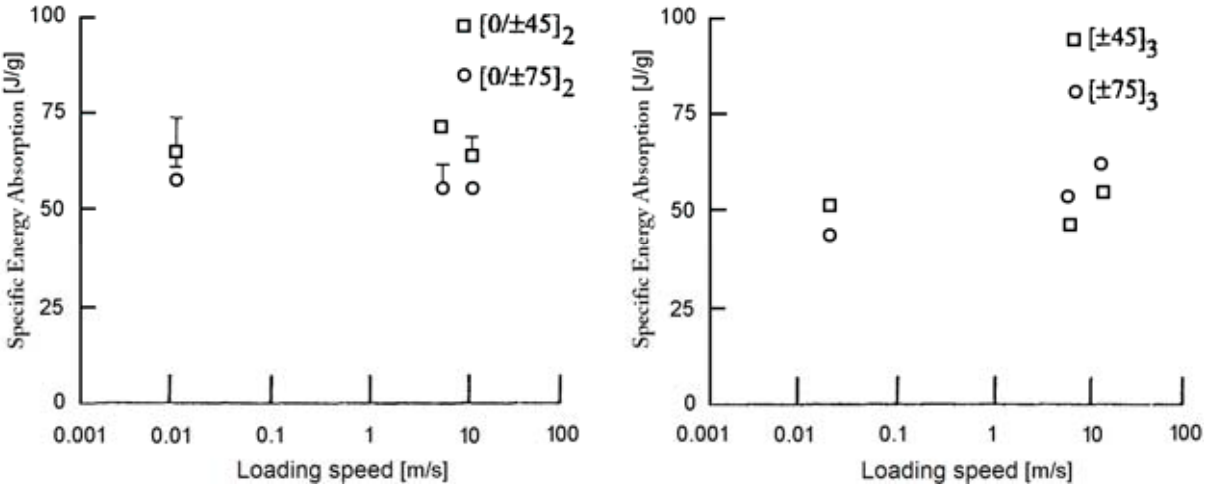

Fig. 19. The influence of strain rates on energy absorption for graphite/epoxy tubes [13]

Our investigations were performed using epoxy composites reinforced with: mat, glass continuous fibres, glass fabric as well as carbon fabric. Glass mat/epoxy composite and glass fabric/epoxy $[(\pm 45)_T]$ structure, both have high viscoelastic proprieties. Glass fabric $[(0/90)_T]_2/0_2/[(0/90)_T]_2$ composite is characterized by large elastic proprieties and low viscoelasticity. The constant loading speed varied widely from 0.01 mm/s to 60 mm/s. The results of this investigation were presented on Fig. 20. For the carbon fabric/epoxy composite the loading rate has a little influence on SEA. High viscoelastic proprieties of the glass/epoxy composite with $[(\pm 45)_T]_6$ fabric and mat reinforcement are a possible explanation for a decrease of SEA with the loading rate growth.

Performed investigations brought the results plotted on Fig. 21. Generally, carbon/epoxy composites are not much sensitive to loading rate changes, while the results of glass/epoxy show a small growth of SEA together with the load ratio increase.

In summary, the impact of strains rates on the EA value is dependent on the composite structure, fibre orientation in plies, laminate sequence and the specimen geometry. Further research of different composite structures behaviour under dynamic loading is indispensable.

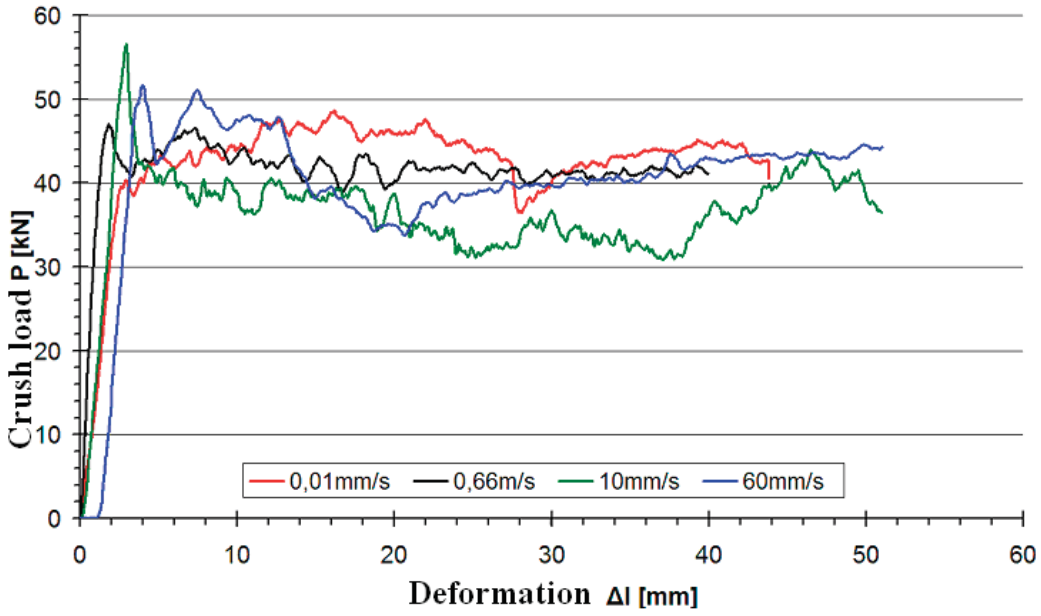

Fig. 20. Load-deformation dependence for the carbon/epoxy composite with $[(0/90)_T]_n$ fabric reinforcement; for different loading speeds. The specimen thickness is equal to 3.3 mm

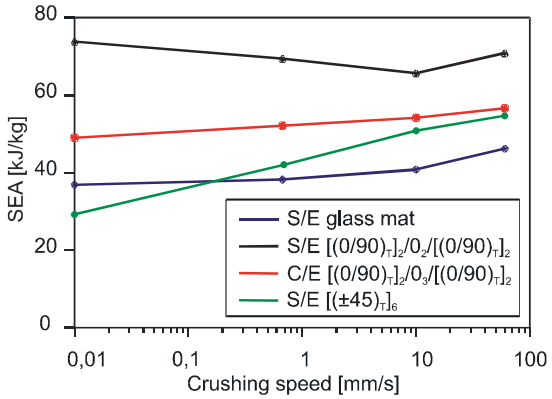

Fig. 21. Dependence of SEA from loading speed for different composite reinforcements

7. Dependence of crush load on deformation obtained in energy-absorption capability tests

Numerical model validations should be based on experimental investigations of progressive crush tests performed on an examined object. Chapter 7 and 8 presents load-deformation dependence (P-Δl) for different absorbing-energy structures.

7.1. Investigations of energy absorption capability of thin-walled rectangular specimens

In this chapter there was presented an experimental research of the energy absorption ability for energy-absorbing polymer composite structures in the shape of a thin-walled rectangle. The analysis obtains the influence of such factors as: fibre and resin type, structure, fibre orientation in ply and the different sequence of various ply structures, as well as the influence of wall thickness on the SEA value.

The specimens had equal shape but different thickness (t). Fig. 22 presents dimensions and the crush initiator design – 45° chamfer. The following composites were investigated:

S/E - glass/epoxy composite with fabric and mat reinforcement,
C/E - carbon/epoxy composite with fabric reinforcement,
A/E - aramid/epoxy composite with fabric reinforcement,
S/PEEK - glass/ polyetheretherketone composite with mat reinforcement,
C/PEEK - carbon/polyetheretherketone composite with fabric reinforcement,
A/PEEK - aramid/polyetheretherketone composite with fabric reinforcement,
S/VE - glass/vinylester composite with fibre reinforcement,
C/VE - carbon/vinylester composite with filament fibre and fabric reinforcement.

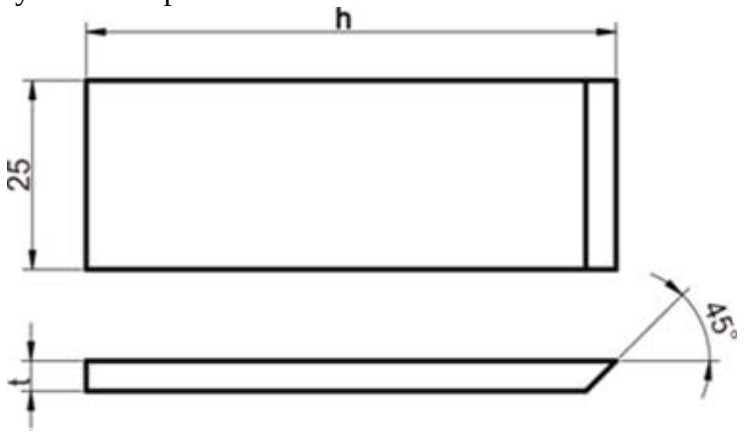

Fig. 22. Dimensions of specimens used in the research

Investigations were performed on the equipment developed in our laboratory, which was described in [14]. It is presented in Fig. 32. It allows examining flat specimens: 25 mm width,

60-80 mm length and 2-8 mm thick. The equipment is installed on a tensile machine. Crushing zone can be observed during the test.

The specimen is installed in the device so that the chamfered edge stands out a little and is in contact with the compressing plate of the stamina machine. The space between guides allows the specimen to move without resistance. The distance between the composite plate and guides is approximately 0.05 mm. Load is applied through a flat follower into the top edge of the specimen. The investigation was performed on tensile machine INSTRON 8802. Dependence of crush load on deformation (specimen shortening) and all over measured values obtained during tests was recorded in PC computer using DAX software.

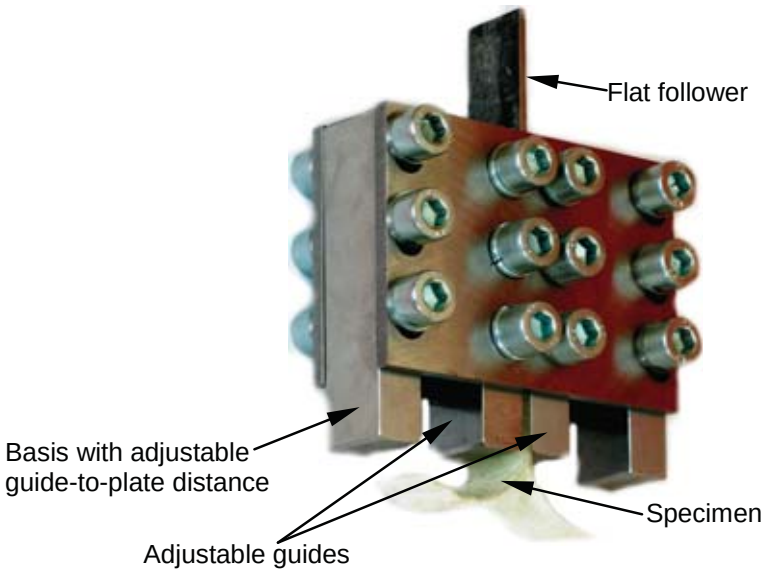

Fig. 23. The device used in test of absorbing-energy ability of composite plates

7.2. The results of the investigation

Fig. 24 presents a relationship P-Δl obtained during examinations. There are four characteristic areas of the curve:

1 - first force peak caused by initiator crush,
2 - second force peak (the force raise until the plate crush into two pieces),
3 - the force fall because of the interlayer cracks occurred,
4 - the area of stable crush.

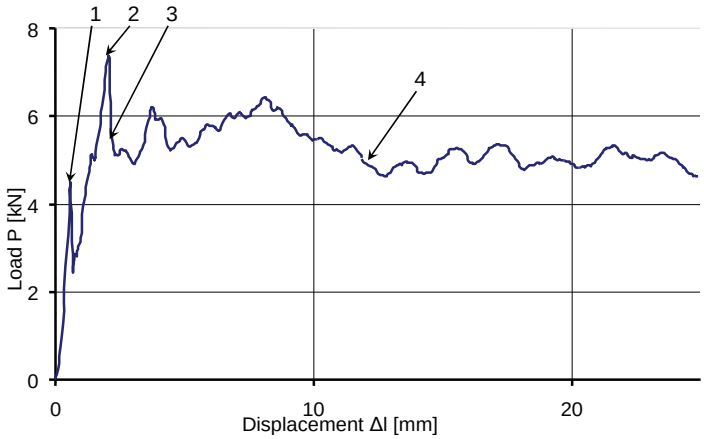

Fig. 24. Typical P-Δl dependence

A detailed specimen description and obtained results were presented in Tab. 2. Fig. 25 shows the specimens prepared to the test. Fig. 26 illustrates progressive crush process while Fig. 27 presents the crushed specimens after the test.

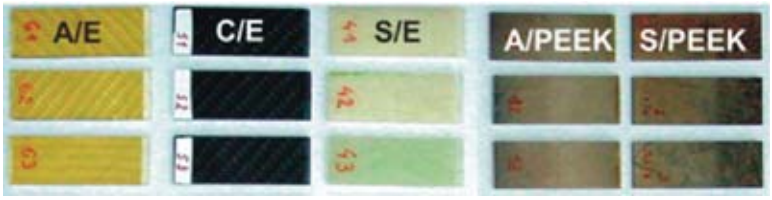

Fig. 25. Specimens prepared to the crush test

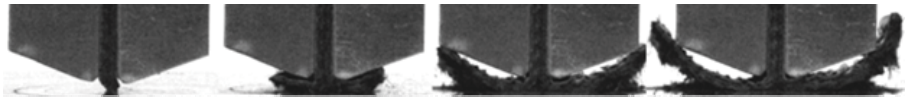

Fig. 26. The progressive crush process

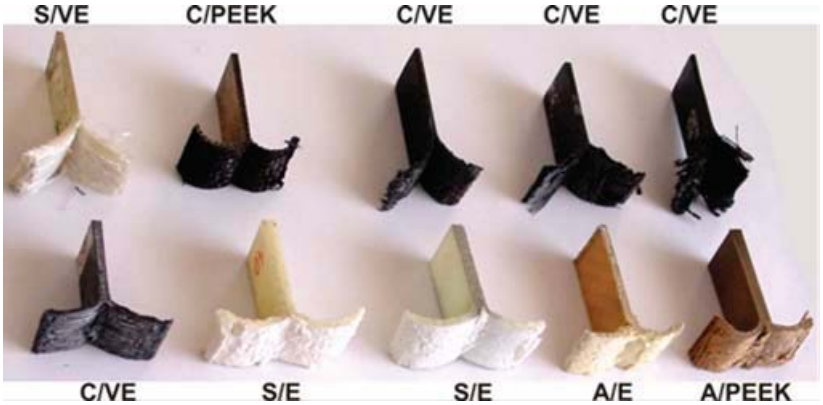

Fig. 27. Specimens after the crush test

Tab. 2. The results of the examination of thin rectangular specimens with different composite type and structures

No.	Composite	Structure	t [mm]	h [mm]	b [mm]	m [g]	z %	P_{max} [kN]	P_{avg} [kN]	$\frac{P_{avg}}{P_{max}}$	EA [J]	SEA [kJ/kg]
5	S/PEEK	mat	3.2	67	25	8.1	0.40	9.9	7.1	0.721	476	58.7
6	S/PEEK	mat	3.2	65	25	7.9	0.40	10.0	7.1	0.711	462	58.4
7	S/PEEK	$[(0/90)_T]_8$	4.6	70	25	11.7	0.42	7.5	5.5	0.735	385	32.9
9	S/PEEK	$[(0/90)_T]_8$	4.6	70	25	11.7	0.42	7.2	4.8	0.669	336	28.7
13	A/PEEK	$[(0/90)_T]_{10}$	4.1	67	25	9	0.35	7.7	5.0	0.653	335	37.2
14	A/PEEK	$[(0/90)_T]_{10}$	4.1	67	25	9	0.35	7.0	5.6	0.800	375	41.7
15	S/E	mat	3.1	75	25	7.5	0.34	5.9	4.0	0.678	299	39.8
18	S/E	mat	3.1	75	25	7.5	0.34	6.68	4.1	0.614	308	41.0
20	S/E	$[(0/90)_T]_8$	3.1	75	25	9	0.58	6.37	4.9	0.769	368	40.8
21	S/E	$[(0/90)_T]_8$	3.1	75	25	9	0.58	6.8	5	0.735	375	41.7
24	S/E	$[(\pm45)_T]_8$	3.1	75	25	9.1	0.58	9.4	6.4	0.681	480	52.7
25	S/E	$[(\pm45)_T]_8$	3.1	75	25	9.1	0.58	11.2	5.6	0.500	420	46.2
27	S/E	mat	4.1	70	25	9.3	0.34	7.3	5.5	0.753	385	41.4
29	S/E	mat	4.1	70	25	9.3	0.34	8	5.7	0.713	399	42.9
32	S/E	$[(0/90)_T]_{12}$	4.1	70	25	11.4	0.59	9	7.7	0.856	539	47.3

34	S/E	$[(0/90)_T]_{12}$	4.1	70	25	11.4	0.59	9.5	8	0.842	560	49.1
35	S/E	$[(\pm45)_T]_{12}$	4.1	70	25	11.4	0.59	9.2	7.7	0.837	539	47.3
38	S/E	$[(\pm45)_T]_{12}$	4.1	70	25	11.4	0.59	9.8	7.7	0.786	539	47.3
40	S/E	mat	5.1	70	25	11.7	0.34	9.3	7.7	0.828	539	46.1
42	S/E	mat	5.1	70	25	11.7	0.34	9.5	7.8	0.821	546	46.7
43	S/E	$[(0/90)_T]_{15}$	5.1	70	25	14.1	0.61	14	11	0.786	770	54.6
46	S/E	$[(0/90)_T]_{15}$	5.1	70	25	14.1	0.61	13.1	11.2	0.855	784	55.6
49	S/E	$[(\pm45)_T]_{15}$	5.1	70	25	14.1	0.61	11.9	9.5	0.798	665	47.2
50	S/E	$[(\pm45)_T]_{15}$	5.1	70	25	14.1	0.61	13.8	9	0.652	630	44.7
52	C/E	$[(0/90)_T]_{10}$	3.2	70	25	7.4	0.44	9.3	7.1	0.763	497	67.2
54	C/E	$[(0/90)_T]_{10}$	3.2	70	25	7.4	0.44	10	7.2	0.720	504	68.1
57	C/E	$[(\pm45)_T]_{10}$	3.2	70	25	7.4	0.44	8.8	7.1	0.807	497	67.2
58	C/E	$[(\pm45)_T]_{10}$	3.2	70	25	7.4	0.44	6.9	5.9	0.855	413	55.8
59	A/E	$[(0/90)_T]_{10}$	3.1	70	25	6.6	0.45	5.7	3.8	0.667	266	40.3
60	A/E	$[(0/90)_T]_{10}$	3.1	70	25	6.6	0.45	4.7	6.1	1.298	427	64.7
63	A/E	$[(\pm45)_T]_{10}$	3.1	70	25	6.6	0.45	7.7	5.8	0.753	406	61.5
65	A/E	$[(\pm45)_T]_{10}$	3.1	70	25	6.6	0.45	7.6	5.9	0.776	413	62.6
66	C/VE	$[(0/90)_T]_7$	2.4	69	25	5.1	0.50	8.3	5.2	0.627	359	70.4
67	C/VE	$[(0/90)_T]_7$	2.4	69	25	5.1	0.50	7.2	4.2	0.583	290	56.8
68	C/VE	$[(0/90)_T]_7$	2.4	69	25	5.1	0.50	6.4	4.4	0.688	304	59.5
69	S/VE	$0/90/\pm45_2/0/90/\pm45_2/90/0$	2.7	66	23.5	5.8	0.60	5.4	2.9	0.544	194	33.5
70	S/VE	$0/90/\pm45_2/0/90/\pm45_2/90/0$	2.7	66	23.5	5.8	0.60	4.5	3.0	0.662	197	33.9
71	S/VE	$0/90/\pm45_2/0/90/\pm45_2/90/0$	2.7	66	23.5	5.8	0.60	4.8	3.2	0.658	209	36.0
72	S/VE	0_9	2.7	66	23.5	6.1	0.60	4.6	4.0	0.859	261	42.7
73	S/VE	0_9	2.7	66	23.5	6.1	0.60	5.5	3.5	0.641	232	38.0
74	S/VE	0_9	2.7	66	23.5	6.1	0.60	5.9	3.6	0.610	238	39.0
75	C/VE	0_9	2.5	66	23.5	5	0.60	8.1	5.2	0.644	345	68.9
76	C/VE	0_9	2.7	66	23.5	5.5	0.60	9.2	5.8	0.630	383	69.6
77	C/VE	0_9	2.7	66	23.5	5.5	0.60	7.5	5.9	0.789	391	71.0
78	C/VE	$0/90/\pm45_2/0/90/\pm45_2/90/0$	3	66	23.5	5.8	0.60	7.1	4.5	0.634	297	51.2
79	C/VE	$0/90/\pm45_2/0/90/\pm45_2/90/0$	3	66	23.5	5.8	0.60	5.4	4.1	0.759	271	46.7
80	C/VE	$0/90/\pm45_2/0/90/\pm45_2/90/0$	3	66	23.5	5.8	0.60	7.0	4.1	0.589	272	46.9
81	C/PEEK	$[(0/90)_T]_{10}$	2.9	66	25	6	0.50	7.2	4.49	0.628	296	49.4
83	C/PEEK	$[(0/90)_T]_{10}$	2.9	66	23.5	6	0.50	5.6	4	0.714	264	44.0

P_{max} - maximum crush load, first peak on curve P-Δl, marking the beginning of crush,
EA - absorbed impact energy, equivalent of the surface under curve P-Δl,
P_{avg} - average load equal to ($P_{avg} = EA/\Delta l_{max}$),
SEA - specific absorbed energy equal to $SEA = EA/m_c$, where m_c is weight of the crushed specimen part,
m - specimen weight,
P_{avg}/P_{max} - index of load uniformity,
t - specimen thickness,
h - specimen height.

Fig. 28-30 present P-Δl dependence for exampled rectangular specimens.

The results presented in Tab. 1 are described with the following quantities:

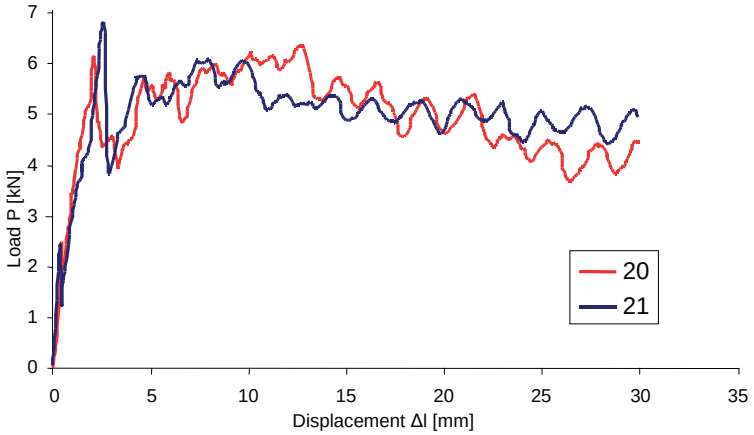

Fig. 28. P-Δl dependence for the glass/epoxy composite with $[(0/90)_T]_8$ structure

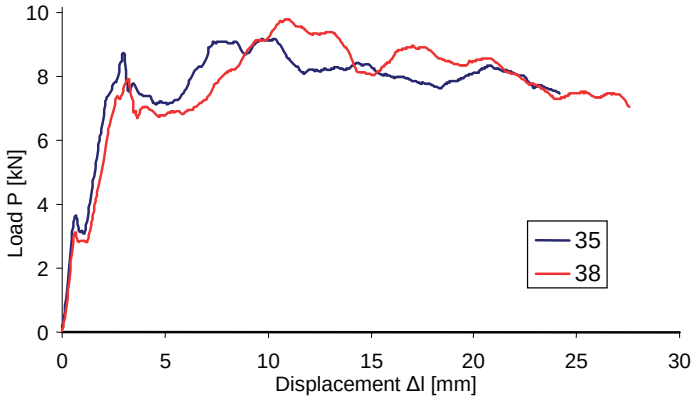

Fig. 29. P-Δl dependence for the glass/epoxy composite with $[(\pm 45)_T]_{12}$ structure

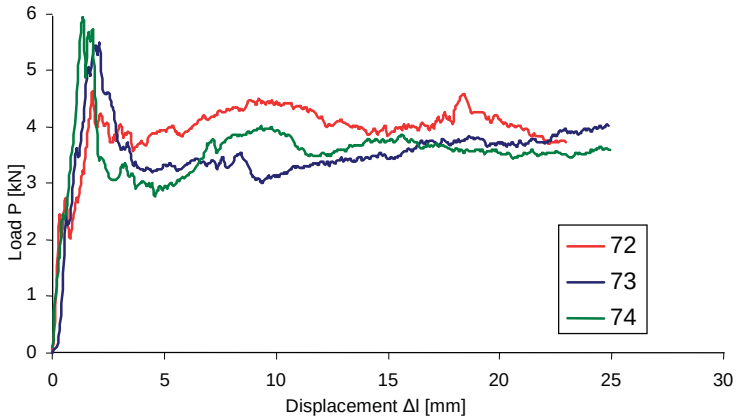

Fig. 30. P-Δl dependence for the glass/vinylester composite with 0_9 structure

Based on the results of performed experiments, the following conclusions were drawn:

- the best energy absorbers are in decrease order: composites with polyetheretherketone, vinylester and epoxy matrix;
- the best reinforcements of the examined composites are: carbon fibres, aramid fibres, which have excellent tensile resistance but very low compressive resistance (absorbed energy constructions are always compressed);
- specimen thickness growth causes increase of the SEA, which was proved for glass/epoxy specimens with both mat and fabric reinforcement.

8. Energy absorption capability for different kind of composite structures of absorbing energy constructions

This chapter presents the results of experimental tests for energy absorbing sandwich structures with different kind of core types: tubes, truncated cones, spherical structures and wavy shells.

8.1. Research of sandwich structures filled with foamed material

Sandwich structures made of composite plates interleaved with foamed material are used in aeronautical engineering frequently. They were investigated in the compressive test to evaluate specific energy absorption. The core was made of non-flammable, foamed polyvinyl chloride, which was stuck in 10 mm packets between 1mm plies of glass/epoxy composite reinforced with $[(0/90)_T]_n$ and $[(\pm 45)_T]_n$ fabric.

Basic mechanical proprieties of the foamed polyvinyl chloride are presented in Tab. 3.

Tab. 3. Mechanical proprieties of the foamed polyvinyl chloride

No.	Mechanical properties		Value	Unit
1	E^+	Tensile elastic modulus	92.43	[MPa]
2	E^-	Compressive elastic modulus	80.63	[MPa]
3	G	Shear elastic modulus	34.0	[MPa]
4	R^+	Tensile resistance	1.82	[MPa]
5	R^-	Compressive resistance	0.911	[MPa]
6	R_S	In-plain shear resistance	1.32	[MPa]
7	ν^+	Tensile Poisson ratio	0.262	-
8	ν^-	Compressive Poisson ratio	0.26	-

Tab. 4. Results of sandwich composite structures with foamed polyvinyl chloride

No.	Composite	Structure	t [mm]	h [mm]	b [mm]	m [g]	P_{avg} [kN]	EA [J]	SEA [kJ/kg]
1	S/E	$[(\pm 45)_T]_n$	44	102	48	29.7	3.7	377	12.7
2	S/E	$[(0/90_T]_n$	44	95	46	26	5.8	551	21.2
3	S/E	$[(0/90_T]_n$	44	95	45	27	5.5	523	19.4
4	S/E	$[(\pm 45)_T]_n$	44	98	45	27	4.1	402	14.9
5	S/E	$[(\pm 45)_T]_n$	44	99	45	26.5	10.7	482	18.2
6	S/E	$[(0/90_T]_n$	44	95	46	28	3.6	342	12.2

where:
t - wall thickness [mm],
h - height [mm],
b - width [mm],
m - weight [g],
P_{avg} - average crush load [kN],
EA - absorbed energy [J],
SEA - specific energy absorbed [kJ/kg].

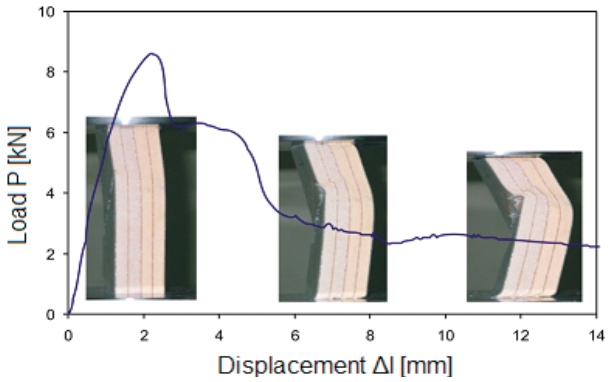

Fig. 31. P-Δl dependence for sandwich structures – item No. 1 in Tab. 4

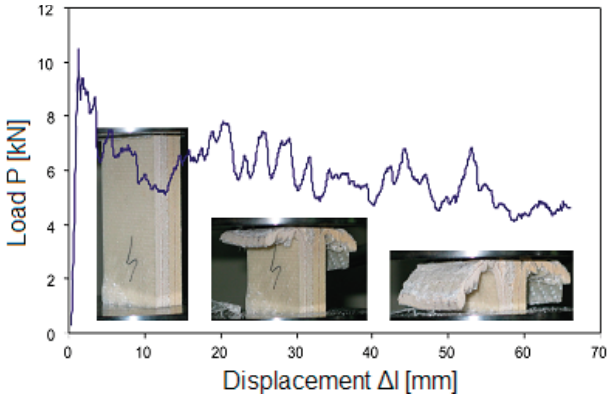

Fig. 32. P-Δl dependence for sandwich structures – item No. 2 in Tab. 4

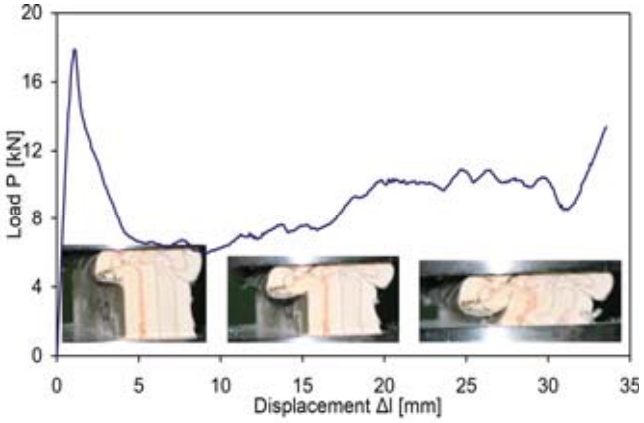

Fig. 33. P-Δl dependence for sandwich structures – item No. 5 in Tab. 4

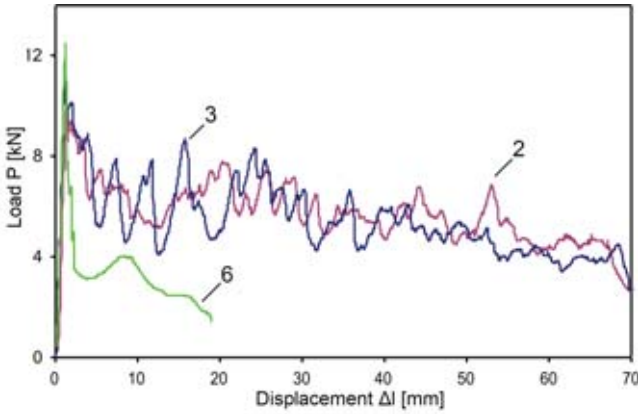

Fig. 34. P-Δl dependence for sandwich structures – items No. 2, 3 and 6 in Tab. 4

The majority of specimens were crushed progressively, as it can be observed on the above graphs, reaching large values of absorbed energy. Sample No. 1 was crushed with global buckling, while sample No. 6 was crushed by global cut, which was the cause of smaller EA result. Unfavourable crush mechanism observed in samples 1 and 6 could be caused by local structure defects or inappropriate specimen geometry. In the case when the larger number of samples would crush by global buckling, the thickness of thin plates should be reduced with non-changed proprieties of foamed material core.

Received results prove, that thin plates made of composite $[(0/90)_T]_n$ revealed larger energy absorption ability than $[(\pm 45)_T]_n$ structure.

8.2. Sandwich structures with tube cores

The examined sandwich structure was consisted of two thin glass/epoxy composite plates with four tube elements fixed between them. The tubes had the following dimensions: length 50 mm and diameter 40 mm. They were made of an epoxy resin with glass matt reinforcement. For comparison purposes, there were also made the following specimen types: one tube made of the same composite filled with foamed material and the structure made of four tubes without foamed material. The fourth kind of specimens was a cylinder made of foamed material, the same that was used to fill other structures.

The specimen parameters and obtained results are presented in Tab. 5. Fig. 5-8 present the results from performed tests.

Tab. 5. Results for sandwich constructions with tube core with and without foamed material

No.	Shape	Composite	Structure	t [mm]	h [mm]	d_{ext} [mm]	m [g]	P_{max} [kN]	P_{avg} [kN]	EA [J]	SEA [kJ/kg]
1	Cylinder	-	Foamed material	-	50.0	38.0	7.4	3.45	1.77	70	11.99
2	Tube with foamed material	S/E	$[mat]_n$	2.0	50.0	40.0	25.8	40.83	21.97	930	42.57
3	Four-tubes structure with FM	S/E	$[mat]_n$	2.0	50.0	40.0	103.2	98.33	72.66	2660	40.51
4	Four-tubes structure	S/E	$[mat]_n$	2.0	50.0	40.0	73.6	3.45	89.29	2590	60.66

where:
d_{ext} - external diameter,
P_{max} - maximum crush load,
EA - absorbed energy [J],
FM - Foamed material filling.

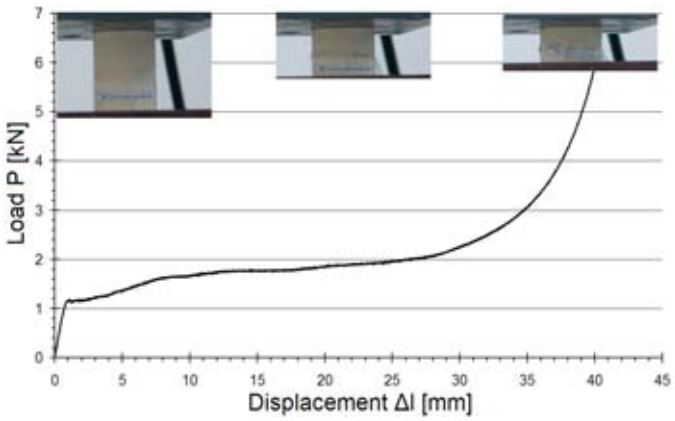

Fig. 35. P-Δl dependence for cylindrical specimens made of foamed material – item No. 1 from Tab. 5

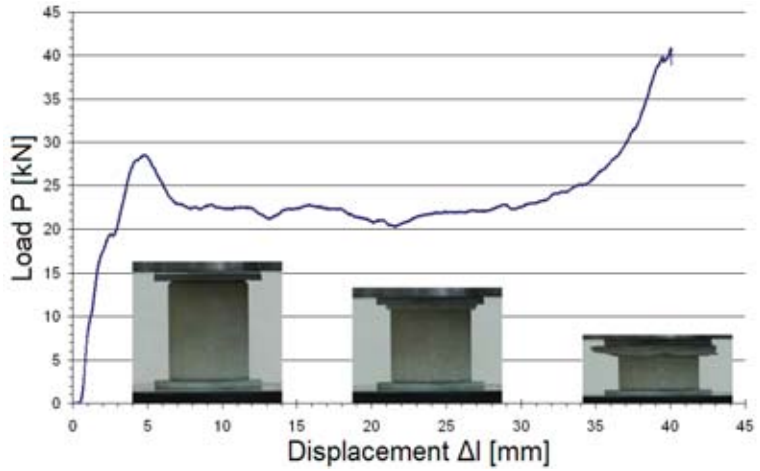

Fig. 36. P-Δl dependence for composite tubes filled with foamed material – item No. 2 from Tab. 5

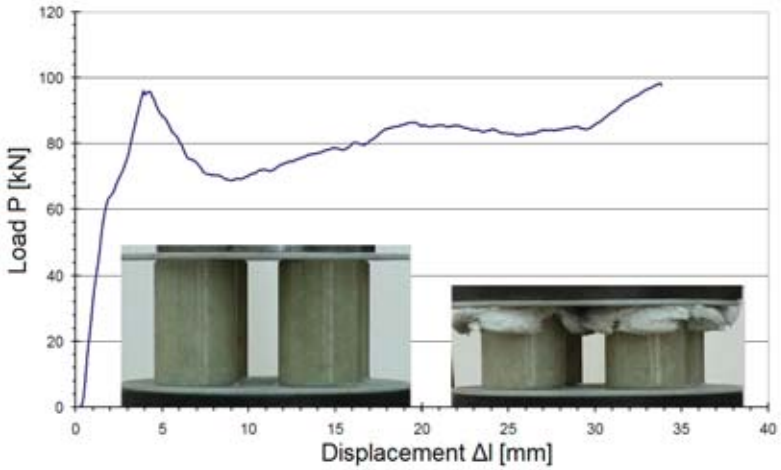

Fig. 37. P-Δl dependence for sandwich structures with core made of four tubes filled with foamed material – item No. 3 from Tab. 5

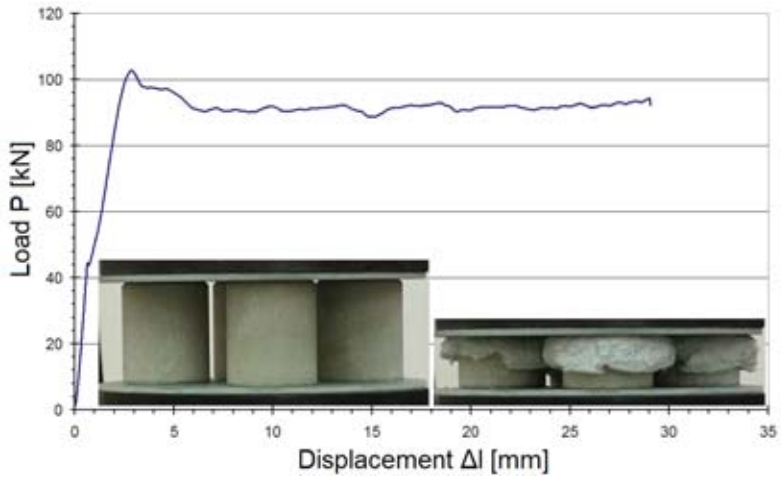

Fig. 38. P-Δl dependence for sandwich structures with core made of four tubes, without foamed material – item No. 4 from Tab. 5

Comparing sample 3 and 4 we can notice that absorbed energy EA for a structure with a filling is only slightly larger than in case of a structure without a filling. Larger weight of sample 3 causes that its SEA is lower. Foamed material does not raise absorbed energy significantly, however SEA is reduced.

The comparison of specimens with one element core (item No. 2) and four-element core (item No. 3) reveals that the Specific Absorbed Energy is approximately on the same level. So, the energy absorbed by single tube has been added up in case of specimen 3.

Foamed material cylinders achieved almost six times lower SEA comparing to the composite structure. On Fig. 35 it is clearly seen that crush load in most part of the curve has small slop what responds to reduction of wormholes inside the specimen. At the end of the curve, when the wormholes are removed, crush load increases rapidly. Energy absorbed by the specimen is very low (equal to 70 J). Regarding very low density of the SEA material, it is comparatively high.

Different crush initiation methods were studied out for sandwich structures with tube cores made of glass mat/epoxy composite. Tube No. 1 was filled with foamed material. On both its sides there were attached flat composite plates. No element for crush initiation was made. Sample No. 2 was made similarly; apart from there was chamfer as a crush initiator made on the top edge of the tube. To attach both facing plates to the core, and not destroy the initiator, the foamed material cylinder was stuck inside the tube on its top part. The plate was attached into this cylinder, so that the initiator was untouched (Fig. 39). In sample No. 3 a notch as the initiator was made in the centre of its height. Tab. 6 presents the results and the specimen description.

Tab. 6. Results for different crush initiation methods

No.	Shape	Composite	Structure	t [mm]	h [mm]	d_{int} [mm]	m [g]	P_{max} [kN]	P_{avg} [kN]	EA [kJ]	SEA [kJ/kg]
1	Tube with FM without initiator	S/E	$[mat]_n$	2.2	93	39.4	92.9	55.2	24.6	1.03	24.62
2	Tube with chamfer	S/E	$[mat]_n$	2.2	93	39.4	62.4	45.9	28.3	1.17	42.18
3	Tube with notch in the middle of height	S/E	$[mat]_n$	2.2	93	39.4	61.9	13.8	16.3	0.66	24.53

where:
d_{int} - internal tube diameter,
FM - foamed material.

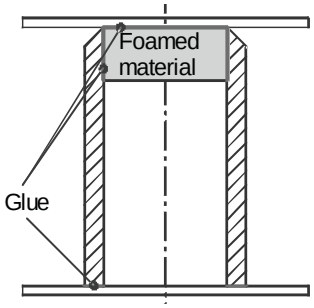

Fig. 39. Fastening of plates with tube cores

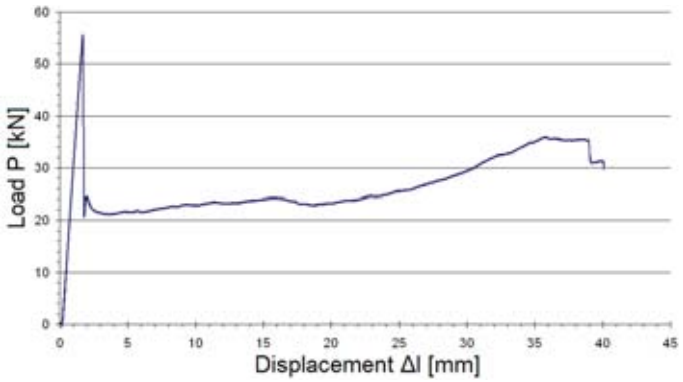

Fig. 40. P-Δl dependence for the tube filled with foam material and without the initiator – item No. 1 from Tab. 6

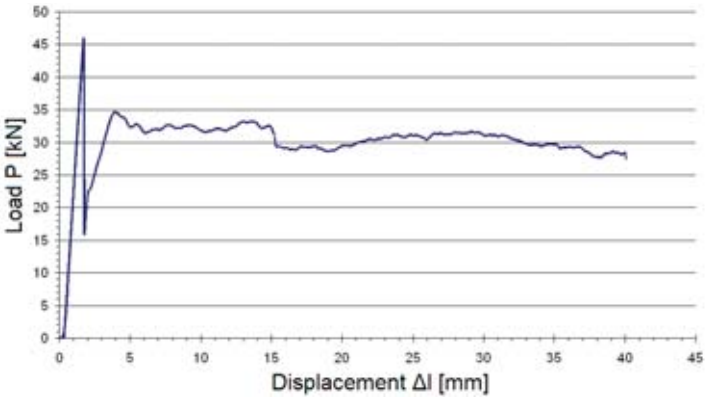

Fig. 41. P-Δl dependence for the tube with chamfer initiator – item No .2 from Tab. 6

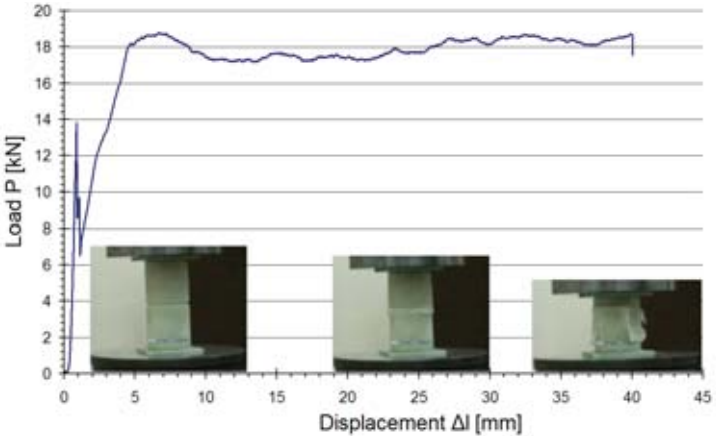

Fig. 42. P-Δl dependence for the tube with centre notch – item No. 3 from Tab. 6

Fig. 40 presents the results of investigations of tubes without any initiator. Their SEA is very low. In the first phase, there is very high force peak, which achieves almost 56 kN. This load causes micro crush in whole volume of the specimen what results in crush load decrease in further part of the curve. The specimens with the initiator in the centre of their height achieved very low SEA, because they crushed catastrophically (Fig. 42). After crush initiation the shear of the specimen occurred.

The most effective way to initiate progressive crush in composite energy absorbing structures is to prepare a chamfer on the edge of the tube as it is presented on Fig. 39. The results of the investigations were presented on Fig. 41.

8.3. Sandwich structures with cores made of truncated cones

In this part sandwich constructions with truncated cones were examined. Tab. 7 presents the results for different configurations. Sample No. 1 was made of a single cone, to which both sides a plate was stuck. The core of sample 2 was consisted of four truncated cones, which were made of epoxy composite with glass mat reinforcement. The cones have the following dimensions: height 75 mm, thickness 2 mm. They were connected to composite plates made of glass fabric/epoxy, which were stuck to their upper and bottom bases.

Tab. 7. Results for sandwich structures with core made of truncated cones

No.	Shape	Composite	Structure	t [mm]	h [mm]	d_{int1} [mm]	d_{int2} [mm]	m [g]	P_{max} [kN]	P_{avg} [kN]	EA [kJ]	SEA [kJ/kg]
1	Cone	S/E	$[mat]_n$	2.2	75.0	56.5	35.3	41.2	30.47	16.20	0.71	29.53
2	Four-cone structure	S/E	$[mat]_n$	2.0	78.0	59.0	31.2	153.5	79.19	65.46	2.97	34.07

Fig. 43 and 44 present compression test curves in conditions of constant crush load rate.

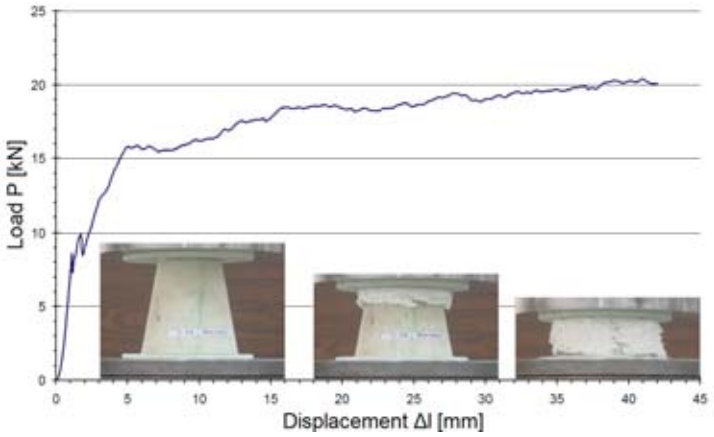

Fig. 43. P-Δl dependence for the single cone – item No. 1 from Tab. 7

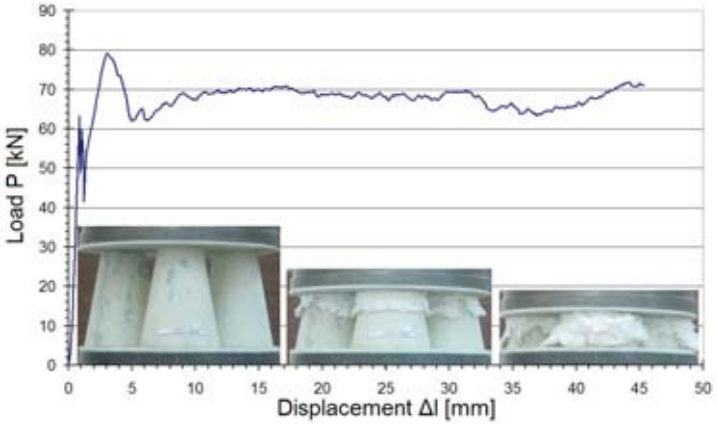

Fig. 44. P-Δl dependence for the sandwich energy absorbing structure with cone core – item No. 2 from Tab. 7

Single cone achieved EA factor equal to 0.71 kJ (Fig. 43). Four-element sandwich structure absorbed 2.97 kJ energy. Obtained SEA is very similar for both specimens. The superposition of absorbed energy for cone elements in the second structure is hold.

8.4. Sandwich structures with spherical cores

Among very different shapes used in energy-absorbing structures, there were also investigated spherical cores. Tab. 8 presents data relating to the examined structures. Specimens No. 1 were made of eight halves of spheres with diameters of 40 mm, from glass/epoxy composite with $[(0/90)_T]_n$ fabric structure. The half-spheres were stuck together in pairs creating 4-element core, to which two bases the composite plates were fixed. Samples No. 2 were made of the same composite. They were consisted of two half-spheres attached to the same plate, on both its sides, opposite to each others. Fig. 45 and 46 illustrate crush process for constant crush load ratio.

Tab. 8. Sandwich structures with spherical core

No.	Com-posite	Structure	t [mm]	h [mm]	d_{int} [mm]	m [g]	P_{max} [kN]	P_{avg} [kN]	EA [kJ]	SEA [kJ/kg]
1	S/E	$[(0/90)_T]_n$	2.9	63.4	39.2	91.0	30.12	13.77	0.52	9.60
2	S/E	$[(0/90)_T]_n$	2.7	65.4	39.5	20.2	20.61	8.52	0.33	27.57
3	S/E	$[(0/90)_T]_n$	2.8	30.1	39.5	10.8	24.01	8.66	0.17	24.21

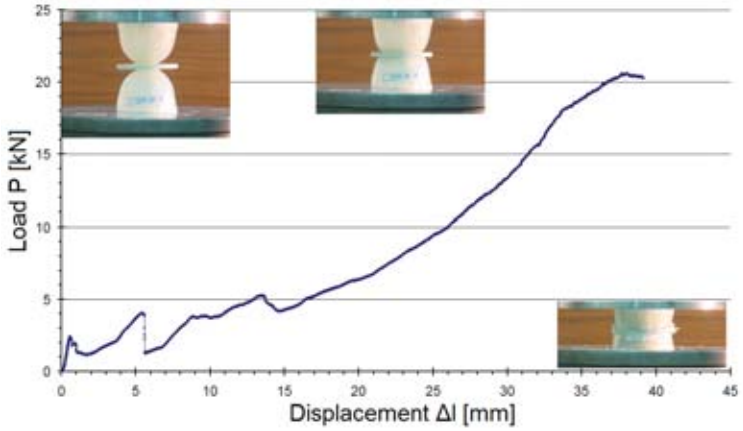

Fig. 45. P-Δl dependence for the sandwich structure with core made of two spheres glued to the common basis – item No. 1 from Tab. 8

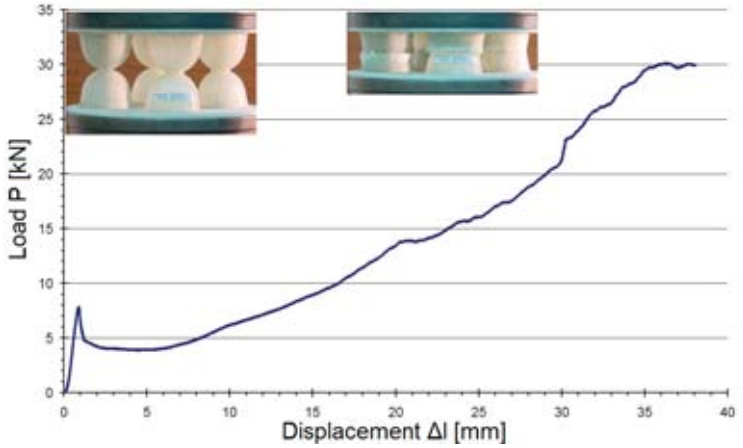

Fig. 46. P-Δl dependence for the sandwich structure with core made of eight spheres – item No. 2 from Tab. 8

During the tests item No. 1 absorbed 0.52 kJ of energy, while the second specimen reached 0.33 kJ. Specific absorbed energy is three times smaller for sample 1 (Tab. 8) than in case of sample 2. This is caused due to the different crush mechanism.

8.5. Sandwich structures with wavy-shell cores

In this section there were examined composites absorbing-energy structures with thin-walled wavy shells, made of epoxy resin with glass mat. They were installed along the edges with facing plates. The results of the test were compared to the results for a single wavy sheath.

The characteristics of the specimens are presented in Tab. 9, while graphs 47 and 48 represent the load-deformation dependence (P-Δl).

Tab. 9. Sandwich structures with wavy shell cores

No.	Composite	Structure	Thick [mm]	High [mm]	Weight [g]	P_{max} [kN]	EA [kJ]	SEA [kJ/kg]
1	S/E	$(\pm 45)_T$	1.6	40.7	28.0	25.09	0.40	27.44
2	S/E	$(\pm 45)_T$	1.7	40.4	24.0	23.48	0.47	32.45
3	S/E	$(\pm 45)_T$	1.7	40.6	22.0	24.70	0.41	31.13
4	S/E	$(\pm 45)_T$	1.7	40.6	24.0	24.31	0.40	28.85
9	S/E	$(0/90)_T$	2.3	57.5	34.0	29.86	0.79	39.16

10	S/E	$(0/90)_T$	1.8	57.5	30.0	29.55	0.70	39.28
11	S/E	$(0/90)_T$	2.2	56.8	32.0	29.41	0.78	40.05
12	C/E	$(0/90)_T$	1.9	39.3	18.0	42.47	0.72	75.79
13	C/E	$(0/90)_T$	1.7	39.5	18.0	38.80	0.67	69.37
14	C/E	$(0/90)_T$	1.7	39.7	18.0	39.95	0.72	74.09
15	C/E	$(0/90)_T$	1.8	39.6	18.0	37.33	0.70	72.29
16	S/E	mat	1.4	57.4	14.0	-	0.13	39.52
17	S/E	mat	1.5	57.4	16.0	-	0.15	38.25
18	S/E	mat (wavy shell group)	1.5	40	80	112.3	1.44	32.3

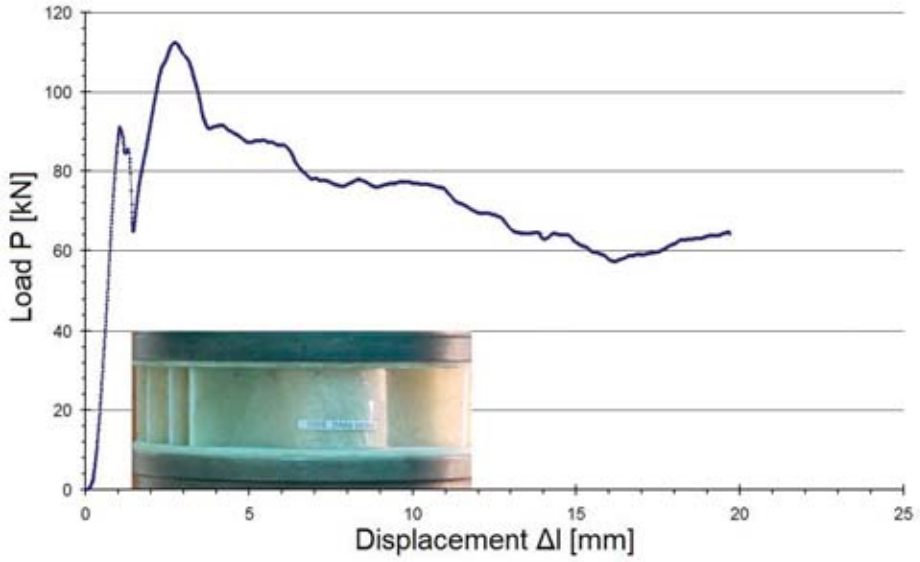

Fig. 47. P-Δl dependence for the sandwich structure with core made of group of wavy shells – item No. 18 in Tab. 9

Sandwich structure with wavy cores had the total length of waves 800 mm. This construction managed to absorb 1.44 kJ, while single specimens with the length of 160 mm absorbed energy equal to 0.15 kJ. For wavy sheaths the rule of adding up the EA is met. Structures made of epoxy resin carbon fabric reinforced reached as double SEA as for the same structures made of glass fabric.

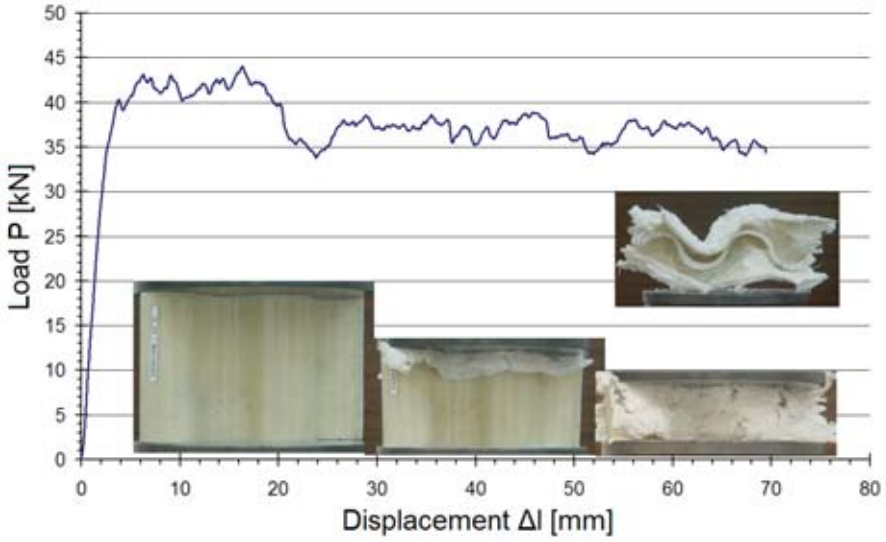

Fig. 48. P-Δl dependence for the single wavy shell – item No. 17 from Tab. 9

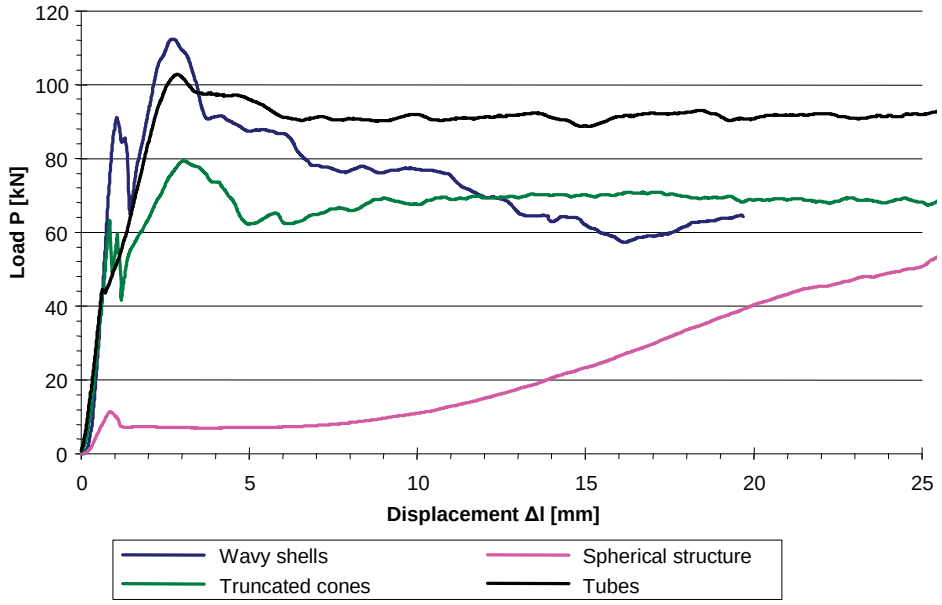

Fig. 49. Comparison of energy absorption ability for different types of the absorbing–energy structures

Fig. 19 presents the comparison of dependence P-Δl for the examined energy absorbing structures. In summary, it has to be noted that sandwich structures made of tubes achieve the largest SEA factor. The next are constructions with cores prepared of truncated cones and then there are cores with wavy shells. The spherical cores achieved the smallest energy absorbing ability. The graphs presented on Fig. 49 do not fully confirm the conclusion presented above because the specimens had different thickness.

8.6. Constructions with cores prepared as cones or tubes with attached spheres

The next part of our work will describe the investigations of composite energy-absorbing structures in which cores made of cones or tubes with half-sphere jointed to their top. The examination covers the test of different kinds of epoxy composite structures: glass mat as well as glass fabric $[(0/90)_T]_n$. Tab. 10 contains the results for given structures. The appropriate load–displacement curves are presented on Fig. 50-59. Items 3 and 6 were filled with foamed material. Whereas specimens No. 4 as well as 7 were prepared with 20 mm cylindrical foamed material inside (see Fig. 39).

Tab. 10. Properties of examined specimens with different core types; with and without foamed material

No.	Shape	Com-posite	Structure	t [mm]	h [mm]	d_{ext} [mm]	d_{ext} [mm]	m [g]	P_{max} [kN]	P_{avg} [kN]	EA [kJ]	SEA [kJ/kg]
1	Cone with sphere	S/E	$[mat]_n$	2.0	95.7	46.26	59.2	40	16.32	11.60	0.87	27.76
2	Tube with sphere	S/E	$[(0/90)_T]_n$	2.3	114.9	39.2	-	48	26.63	17.95	1.43	42.93
3	Tube with FM	S/E	$[(0/90)_T]_n$	2.2	115.0	39.2	-	68	25.78	17.07	1.31	28.87
4	Tube with 2 cm FM	S/E	$[(0/90)_T]_n$	2.0	90.0	39.2	-	40	24.44	18.97	1.16	42.74
5	Tube with sphere	S/E	$[mat]_n$	2.3	115.8	39.2	-	47	19.86	13.60	1.07	33.51
6	Tube with sphere +FM	S/E	$[mat]_n$	2.4	117.0	39.2	-	62	19.16	12.86	1.04	24.42
7	Tube with 2 cm FM	S/E	$[mat]_n$	2.4	89.7	39.2	-	38	19.24	13.84	0.98	32.95

FM – Foamed material filling

Tab. 11. Results for specimens in shape of tubes and cones joint with half-sphere structures

No.	Structure	Com-posite	Structure	t [mm]	h [mm]	d_{ext} [mm]	d_{ext} [mm]	m [g]	P_{max} [kN]	P_{avg} [kN]	EA [kJ]	SEA [kJ/kg]
1	Tube with sphere four- element structure	S/E	$[mat]_3$	1.9	111.8	39.2	-		56.18	41.4	2.90	30.23
2	Tube with sphere four- element structure	S/E	$[(0/90)_T]_3$	2.0	115.2	39.2	-	179.0	81.28	61.6	4.61	39.65
3	Cone with sphere four- element structure	S/E	$[mat]_3$	1.8	96.0	45.5	59.2	158.0	60.93	46.4	3.26	28.16

Tab. 12. Comparison of structures with spheres for single and four element cores

No.	Structure	Com-posite	Structure	P_{max} [kN]	P_{avg} [kN]	EA [kJ]	SEA [kJ/kg]	P_{avg4}/P_{avg1}	EA_4/EA_1
1	Cone with sphere	S/E	$[mat]_3$	16.32	11.60	0.87	27.76	-	-
2	Cone with sphere four-element structure	S/E	$[mat]_3$	60.93	46.37	3.26	28.16	4.0	3.7
3	Tube with sphere	S/E	$[mat]_3$	19.86	13.60	1.07	33.51	-	-
4	Tube with sphere four-element structure	S/E	$[mat]_3$	56.18	41.40	2.90	30.23	3.0	2.7
5	Tube with sphere	S/E	$[(0/90)_T]_3$	26.63	17.95	1.43	42.93	-	-
6	Tube with sphere four-element structure	S/E	$[(0/90)_T]_3$	81.28	61.60	4.61	39.65	3.4	3.2

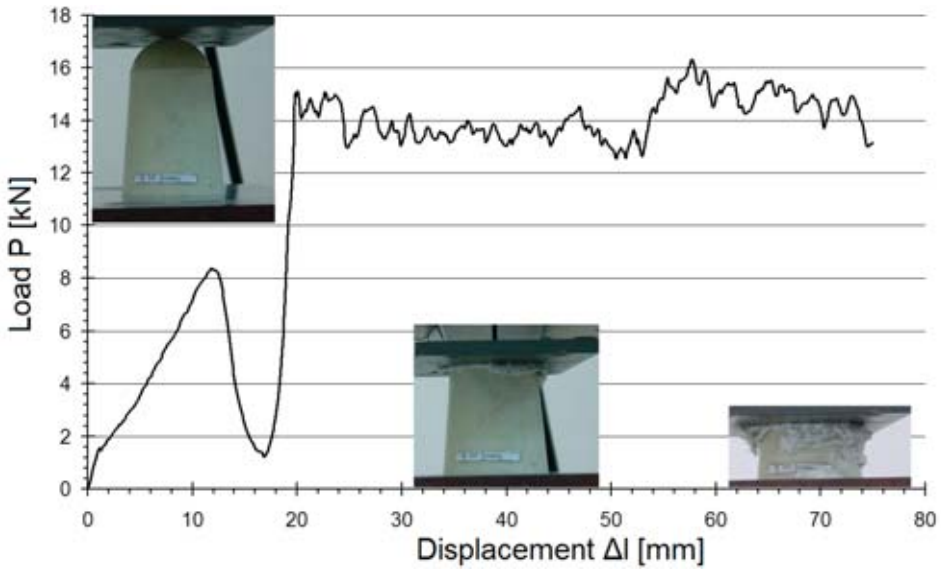

Fig. 50. P-Δl dependence for the tube-with-cone structure made of glass mat with epoxy resin – item No. 1 from Tab. 10

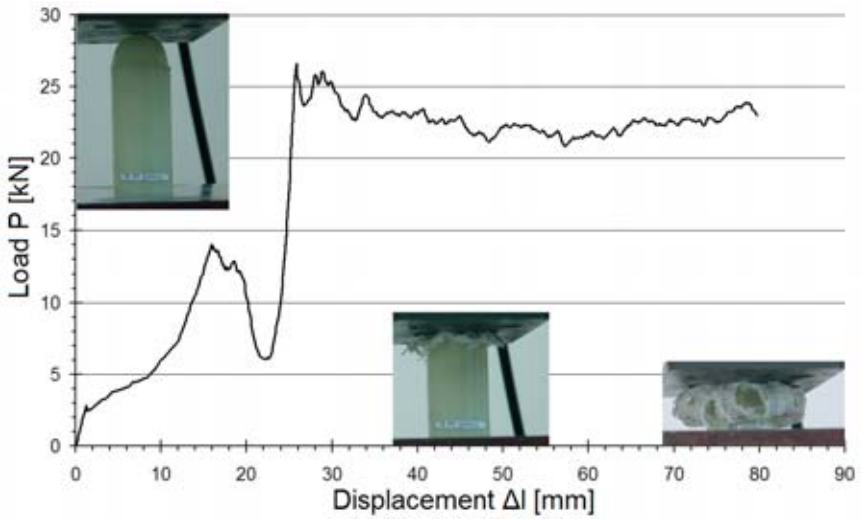

Fig. 51. P-Δl dependence for the tube-with-sphere structure made of glass fabric with epoxy resin – item No. 2 from Tab. 10

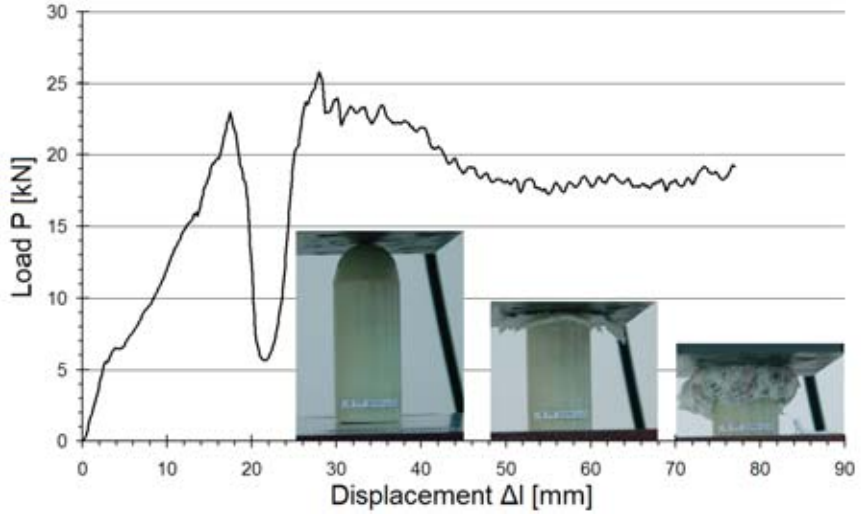

Fig. 52. P-Δl dependence for the tube-with-sphere structure made of glass fabric with epoxy resin and filled with foamed material – item No. 3 from Tab. 10

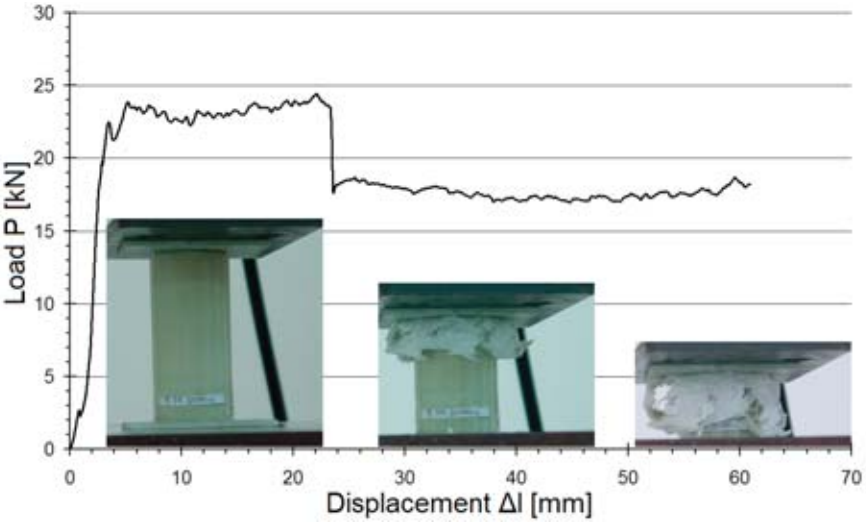

Fig. 53. P-Δl dependence for the tube-with-sphere structure made of glass fabric with epoxy resin and two-centimetre foamed material cylinder inside – item No. 4 from Tab. 10

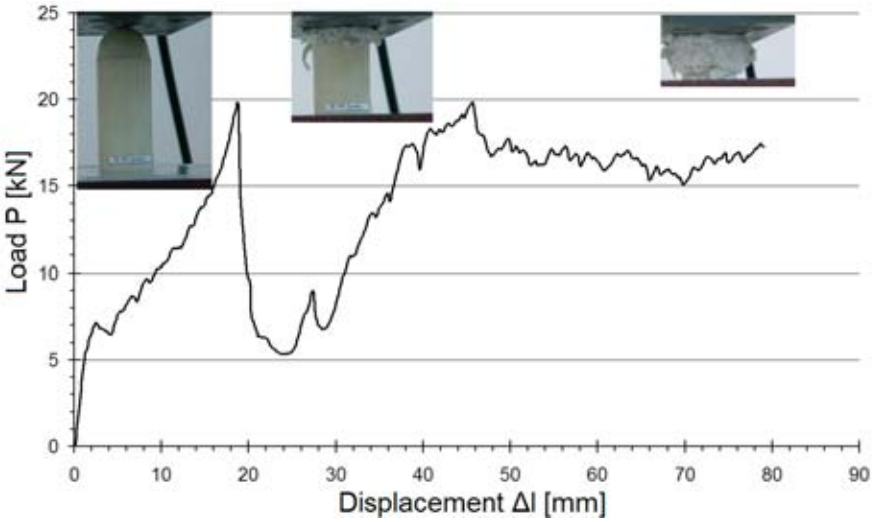

Fig. 54. P-Δl dependence for the tube-with-sphere structure made of glass mat with epoxy resin – item No. 5 from Tab. 10

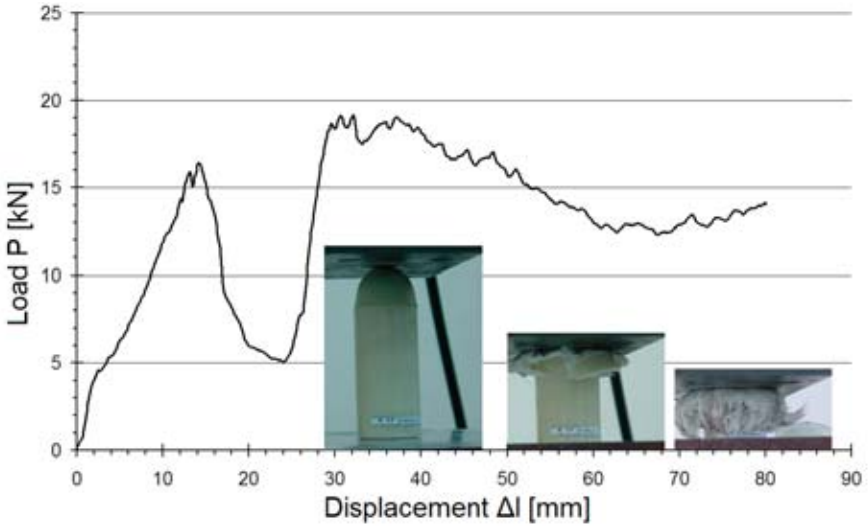

Fig. 55. P-Δl dependence for the tube-with-sphere structure made of glass fabric with epoxy resin and filled with foamed material – item No. 6 from Tab. 10

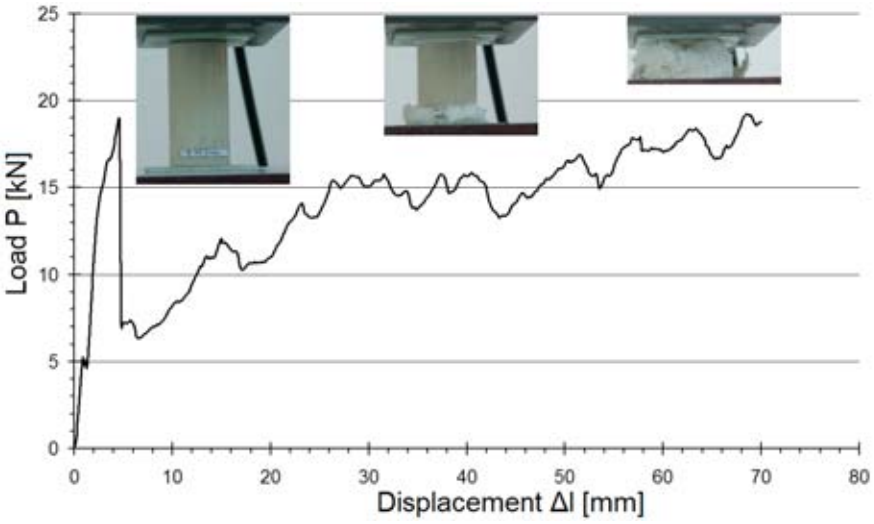

Fig. 56. P-Δl dependence for the tube-with-sphere structure made of glass mat with epoxy resin and two-centimetre foamed material cylinder inside – item No. 7 from Tab. 10

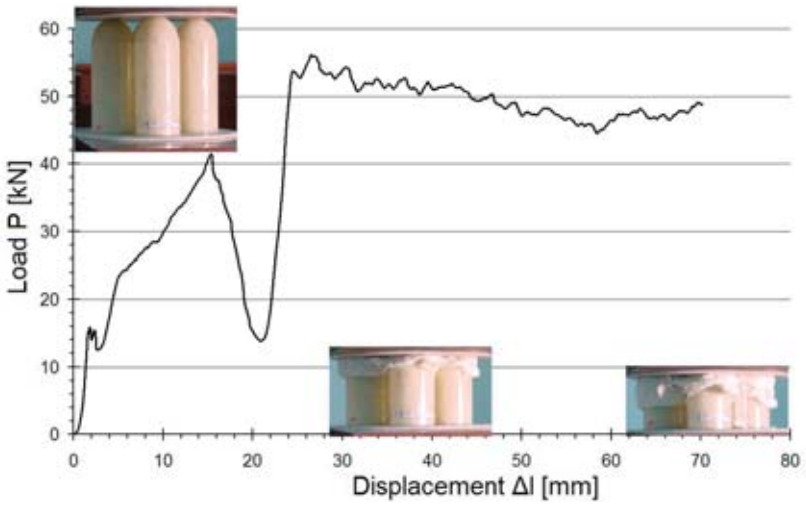

Fig. 57. P-Δl dependence for the tube-with-sphere sandwich structure made of glass mat with epoxy resin – item No. 1 from Tab. 11

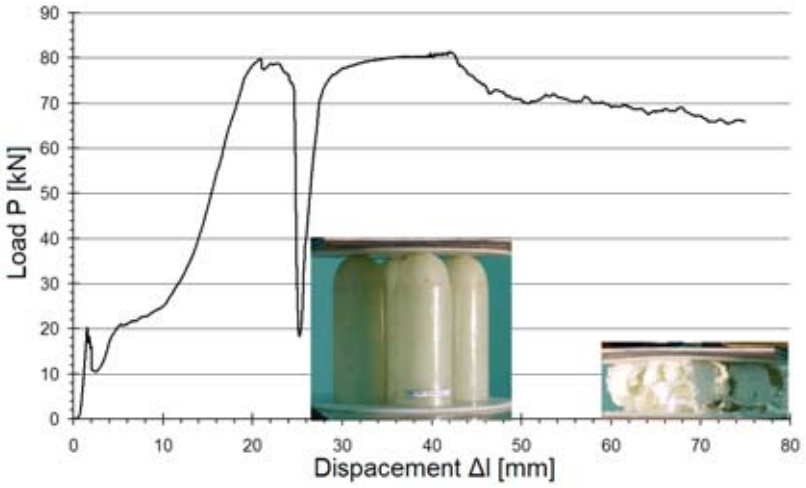

Fig. 58. P-Δl dependence for the tube-with-sphere sandwich structure made of glass fabric with epoxy resin – item No. 2 from Tab. 11

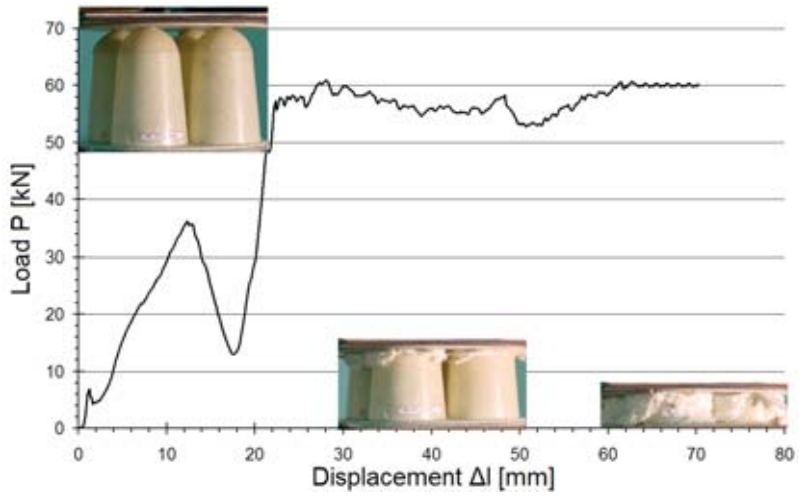

Fig. 59. P-Δl dependence for the cone-with-sphere sandwich structure made of glass mat with epoxy resin – item No. 3 from Tab. 11

On the presented graphs it is clearly seen that the joint between tube/cone with sphere is distinctly marked on the curves. The curves are composed of two parts. The first part is identical as in case of sphere structures crush. The second part has a shape identical as for tubes or cones loading. At the point of the tube/cone-sphere joint, force decrease is fast followed by its rapid growth. The fastening reduces the strength of the whole structure. The sphere is pressed into the tube (or cone), the joint is cut and then the crushed sphere is bending inside the tube (or cone) under a very low impact. Then the crush load grows, which is caused by progressive crush of the element, despite lack of any initiator. In the first phase of tubes (cones) crush there are no clear load peaks.

9. Summary

Comparing identically prepared specimens (Tab. 9) it can be observed that SEA obtained by carbon fibre composite is very far larger than glass fabric composite. Comparing the influence of core shape: tube absorbs more impact energy than cones. The difference is small because the cone had a small slop of the element of the cone.

Foamed material filling of the specimens brings only a very little increase of absorbed energy, however, due to a weight increase it reduces SEA. For tubes with sphere cover made of glass mat the filling reduces SEA by about 33%, for glass fabric reinforcement the lowering is equal to 22%. 20 mm foamed material cylinder inside the specimens No. 4 and 7 practically has no influence on the results.

Now we will discuss the relationship between absorbing-energy sandwiches with four-element cores made of tubes/cones joined with spheres. Tab. 9 presents properties of these structures. In accordance to the expectations, the largest SEA was reached for a structure built from glass fabric reinforcement, while the smallest SEA was noted in case of a glass mat composite. Tubes with spheres exhibit larger SEA than cones with spheres. Comparing single-element and sandwich four-element structures presented in Tab. 10 allows to conclude that the superposition of absorbed energies for single elements holds. Specific absorbed energy remains at the same level.

Foamed material filling of energy-absorbing elements causes an increase of the absorbed energy in those cases when the core element wall is thin. This prevents from local buckling.

Based on the results of all performed investigations, the following summary conclusions were made:

- the mechanical properties of composites, such as elastic modulus, resistance needed in numerical model development, should be determined experimentally for strain rates corresponding to operating conditions of the structure.
- fibrous composites have numerous strength hypotheses, which take into account different factors like: tensile strength, compressive strength, orthotropic structure and general anisotropic structure. Appropriate investigations can help to choose the hypothesis which describes given composite best.
- the influence of the matrix (the resin) on SEA is significant. Mechanical properties of utilized matrix play an important role in an energy-absorbing process, especially their crack propagation resistance. A brittle matrix, like polymer resins, performs smaller ability of energy absorption. PEEK matrix reached the largest SEA values.
- friction forces play a very important part in progressive crush process of the polymer composites. Some scientists state that the friction forces absorb about 40% of impact energy, therefore they should be taken into account in numerical model development.
- influence of strain rates on amount of absorbed energy in progressive crush is not clearly defined. Some scientists show a gain of energy absorption with strain rates increase, others present the opposite results. In some researches there is no dependence between a strain rate and the amount of energy absorbed by composite structures. Our results are shown in Fig. 21. Carbon composites are not sensitive to load rates, whereas the insignificant growth of SEA glass composites can be observed.

Bibliography

[1] Ochelski, S., *Ocena kompozytowych elementów konstrukcji energochłonnej obciążonej dynamicznie*, Wyd. WAT (Rozdział 15 monografii pt. Analizy numeryczne wybranych zagadnień mechaniki), pp. 292-314, Warszawa 2007.

[2] *Fibre Reinforcements for Composite Material*, Composite Material, Vol. 2, New York-Tokyo 1988.

[3] Ochelski, S., *Dynamiczna wytrzymałość kompozytów polimerowych*, Rozprawy Inżynierskie, 38 (1), pp. 73-92, 1990.

[4] Ochelski, S., *Metody doświadczalne mechaniki kompozytów konstrukcyjnych*, WNT, Warszawa 2004.

[5] Falenkov, A., Wabakin, A., Mansurov, R., Stiepanov, P., Malinin, N., *Kryteria procnosti stiekloplastika s kososloinym armirowanijem*, Mehanika kompozitnyh Matierialov, 1985.

[6] Teters, G., Upitis, Z., *Mehanoljuminiescencija rannih i predielnyh stadii razrušenija stiekloplastika*, Mehanika Kompozitnyh Matierialov, 1987.

[7] *Strukture des composites essais mecaniques des composites fibres/resine*, Ed.: Krawczak, P., de Douai, dept Technologie des Polymeres et Composites, 1996.

[8] Tohgo, K., Wang, A., Chou, T., *A Criterion for Splitting Crack Initiation in Unidirectional Fibre-Reinforced Composites*, J. Composite Materials, Vol. 27, No. 11, pp. 1055-1075, 1993.

[9] Byun, J., Gillespie, J., Chou, T., *Mode I Delamination of a Three-dimensional Fabric Composite*, J. Composite Materials, Vol. 24, pp. 497-518, 1990.

[10] Mall, S., Yun, K., Kochhar, N., *Characterization of Matrix Toughness Effect on Cyclic Delamination Growth in Graphite Fibre Composite*, Composite Materials: Fatigue and Fracture, Vol. 2, 1989.

[11] Morka, A., Niezgoda, T., Kiczko, A., Gotowicki, P., *Numeryczna i doświadczalna analiza procesu delaminacji i struktury kompozytu polimerowego*, XI Krajowa Konferencja Naukowo-Szkoleniowa Mechaniki Pękania, Kielce/Cedzyna 2007.

[12] Mamalis, A., Manolakos, D., Demosthenous, G., Ioannidis, M., *Axial Collapse of Thin-Walled Fibreglass Composite Tubular Components at Elevated Strain Rates*, Composites Engineering, Vol. 4, No. 6, pp. 653-677, 1994.

[13] Farley, G., Jones, R., *Energy-Absorption Capability of Composite Tubes and Beams*, 1989.

[14] Starbuck, J, M., Simunovic, S., Jacob, G, C., *Test Methodologies for Determining Energy Absorbing Mechanisms of Automotive Composite Materials Systems*, Proc. 2000 Future Car Congress, Arlington, VA, USA 2000.

"The author's reward was sponsored by Society of Collective Management of Copyrights of Creators of Scientific and Technical Works KOPIPOL with registered office in Kielce with duties obtained on the ground of the art. 20 and art. 20^1 of law on copyrights and related rights."